



HAL
open science

Amphiphilic Polymeric Nanoreactors Containing Rh(I)-NHC Complexes for the Aqueous Biphasic Hydrogenation of alkenes

Sasaline Salomon Sambou, Roman Hromov, Illia Ruzhylo, Hui Wang, Audrey Allandrieu, Cassandra Sabatier, Yannick Coppel, Jean-Claude Daran, Florence Gayet, Agnès Labande, et al.

► To cite this version:

Sasaline Salomon Sambou, Roman Hromov, Illia Ruzhylo, Hui Wang, Audrey Allandrieu, et al.. Amphiphilic Polymeric Nanoreactors Containing Rh(I)-NHC Complexes for the Aqueous Biphasic Hydrogenation of alkenes. *Catalysis science and Technology*, 2021, 11, pp.6811-6824. 10.1039/D1CY00554E . hal-03171897

HAL Id: hal-03171897

<https://hal.science/hal-03171897>

Submitted on 29 Sep 2021

HAL is a multi-disciplinary open access archive for the deposit and dissemination of scientific research documents, whether they are published or not. The documents may come from teaching and research institutions in France or abroad, or from public or private research centers.

L'archive ouverte pluridisciplinaire **HAL**, est destinée au dépôt et à la diffusion de documents scientifiques de niveau recherche, publiés ou non, émanant des établissements d'enseignement et de recherche français ou étrangers, des laboratoires publics ou privés.

Amphiphilic Polymeric Nanoreactors Containing Rh(I)-NHC Complexes for the Aqueous Biphasic Hydrogenation of Alkenes

Sasaline Salomon Sambou,^a Roman Hromov,^a Illia Ruzhylo,^a Hui Wang,^a Audrey Allandrieu,^a Cassandra Sabatier,^a Yannick Coppel,^a Jean-Claude Daran,^a Florence Gayet,^a Agnès Labande,^{*a} Eric Manoury^{*a} and Rinaldo Poli^{*a,b}

A rhodium(I) complex bearing a monodentate N-heterocyclic carbene ligand has been confined into the core of amphiphilic polymeric core-crosslinked micelles (CCMs). The Rh complex was covalently bound to the polymeric chains by incorporation of a polymerizable unit on the NHC ligand. Nanoreactor Rh-NHC^{mes}@CCM **5b** has been evaluated as catalyst for the aqueous biphasic hydrogenation of styrene and other alkenes. It has shown a high activity with styrene at low catalytic loading (10 000/1 substrate/Rh ratio), greater than the analogous molecular Rh(I) complex, and its evolution to Rh⁰ is slower. This is attributed to several factors, among which the confinement effect and the favourable polyoxygenated environment of the nanoreactor core. Finally, the CCM could be recycled up to four times with almost no loss of activity over 3 h cycles and the loss of rhodium per cycle was on average inferior to 0.6 ppm.

Introduction

The recovery and recycling of catalysts have become essential prerequisites, for industrial applications, to improve energetic efficiency, limit the environmental footprint and lower the cost, especially when rare metals and expensive ligands are involved.^{1, 2} One of the successful strategies for recycling is biphasic catalysis in which two immiscible liquid phases are used.³ One of them dissolves the catalyst and the other one is composed of the substrate(s) and product(s) or their solution in a suitable solvent and they can be easily separated by simple decantation. Although the use of fluorinated organic solvents^{4, 5} and ionic liquids^{6, 7} for catalyst confinement has attracted a great deal of attention, water remains the most interesting choice from the ecological and economical points of view.⁸⁻²⁰ An interesting approach to aqueous homogeneous biphasic catalysis is the use of amphiphilic core-shell crosslinked copolymers. Their hydrophobic part (core), which contains the catalyst, serves as a place of exchange between reagents/products, while the hydrophilic part (shell) ensures the compatibility and stability of the macromolecule in the aqueous phase, thus facilitating the separation, recycling and recovery of the catalyst. These polymeric structures present many advantages compared to classical micelles,²¹⁻²³ such as the absence of an equilibrium with free amphiphilic non-crosslinked arms, leading to lower polymer and catalyst losses. The use of polymeric structures with controlled architecture as catalytic supports is an emerging area.²⁴ As early as 2003, a phosphine-functionalized core-shell polymer was prepared by Sawamoto *et al.* by [RuCl₂(PPh₃)₃]-catalysed atom-transfer radical polymerization (ATRP) and was successfully applied to Ru-catalysed oxidation of alcohols.²⁵ Although catalytic activity was lower with these functionalized polymers than with molecular species, an inverse correlation between catalyst loading in the polymeric structure and activity was observed. O'Reilly *et al.* have developed shell-crosslinked amphiphilic micelles (SCMs) containing copper(I) coordinated to terpyridine ligands.²⁶ These crosslinked micelles were used as catalysts in Huisgen-type cycloadditions. The same team has also reported highly efficient organocatalytic nanoreactors for acylation reactions of hydrophobic substrates in aqueous media. The

outstanding reactivity compared to that of catalysis in regular organic solvents was explained by the hydrophobic environment in the core of the nanoreactors and the high local organocatalyst concentration.²⁷ SCMs containing Co(III)-salen-functionalized hydrophobic cores were prepared by Weck *et al.* in 2011.²⁸ In their case, the crosslinking was carried out by UV irradiation. In the hydrolytic kinetic resolution of epoxides, these nanoreactors exhibited a substrate selectivity based on hydrophobicity: the higher the hydrophobicity, the better the conversion. Interestingly, these nanoreactors could be recycled up to 7 times by ultrafiltration, without drop in activity or enantioselectivity. Finally, Zheng *et al.* described the synthesis of Ru-containing core-crosslinked micelles (CCMs) and their use as photocatalysts for the aerobic oxidation of sulfides.²⁹ Again, these CCMs could be efficiently recycled by ultrafiltration and reused up to three times. None of the above polymer-supported catalysts, however, was implemented under aqueous biphasic conditions.

We have been interested for some time in the synthesis and aqueous biphasic catalytic applications of core-crosslinked micelles (CCMs), obtained by crosslinking of linear amphiphilic polymers after their self-assembly as micelles.³⁰⁻³⁷ Recently, phosphine ligand-functionalized CCMs have been developed in our group and applied successfully in several Rh-catalysed reactions, i.e. the biphasic hydroformylation of 1-octene^{30, 31, 34, 36} and hydrogenation of styrene and 1-octene.³³ However, several issues are associated with the use of phosphines such as their propensity to get oxidized and their lability when coordinated to Rh^I, which leads to macrogelation for small P/Rh ratios.³³ N-heterocyclic carbenes (NHCs) are often considered as phosphine surrogates, although their σ -donor character is often more pronounced and their π -acceptor character is weaker – at least for imidazol-2-ylidenes.³⁸⁻⁴³ The latter are easily synthesized from inexpensive, commercially available starting materials, via imidazolium salts.⁴⁴ They generally, if not always, form very strong bonds with many transition metals and thus often give air-stable, easy-to-handle complexes with non-labile metal-ligand bonds. They are now widely used in catalysis and can often surpass phosphines in terms of activity.⁴⁵⁻⁴⁷

In 2004, Weberskirch *et al.* presented the first example of an NHC-Rh catalyst incorporated in an amphiphilic, water-soluble block copolymer (Fig. 1, top).⁴⁸ This macrocatalyst was

successfully used for the aqueous biphasic hydroformylation of 1-octene, with an excellent phase separation and a very low rhodium leaching (0.4 ppm), showing the robustness of the Rh-NHC bond. However, the yield over a 2h cycle was only 43% and when the reaction time was prolonged to 18 h, hydrolysis of ca. 25% of the ester bonds was observed. More recently, Taton *et al.* developed NHC-containing star-like polymeric nanocatalysts, synthesized by RAFT polymerization.^{49, 50} The “macroarms” were assembled by deprotonation of the benzimidazolium precursors and their subsequent coordination to a palladium centre, which served as crosslinking reaction and stabilized the whole star-like structure (Fig. 1, bottom). These Pd-NHC nanocatalysts were used for the Suzuki-Miyaura coupling of 4-iodotoluene with 4-(hydroxymethyl)phenylboronic acid under aqueous conditions. A strong, positive confinement effect on catalytic activity was observed compared to an analogous molecular catalyst. This was associated with a very low Pd leaching, and contrarily to what is usually observed with Pd-NHC molecular catalysts in water, no Pd nanoparticles were observed in the nanostructures. However, the authors also observed an increase in size of their nanocatalysts after the first run, which probably indicated a reorganization of the polymeric structure. Since the publication of these two notable examples, a growing number of contributions on the use of NHC-containing polymeric catalysts has been reported, confirming the unquestioned potential of NHC ligands for catalysis.⁵¹⁻⁶⁰ However, polymer-supported NHC-metal catalysts with a controlled core-shell architecture are limited to only one example,⁵³ to the best of our knowledge.

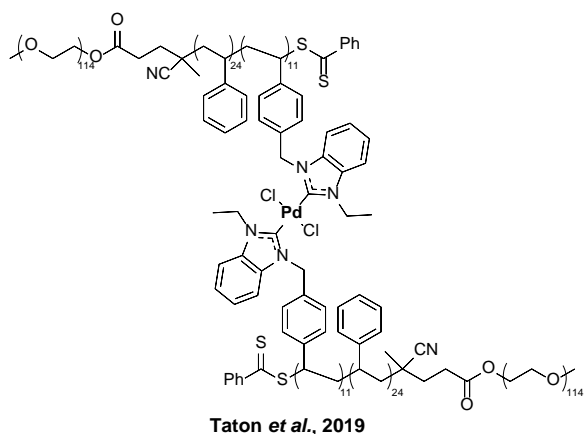
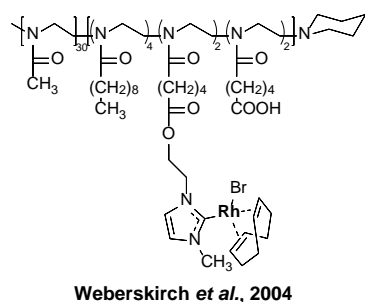


Figure 1. [NHC-Rh]-containing amphiphilic, water-soluble macroligand by Weberskirch *et al.* (2004, top).⁴⁸ Pd-based star-like polymeric nanocatalyst by Taton *et al.* (2018, bottom).⁵⁰

In view of the previous results with phosphine-containing CCM nanoreactors (Fig. 2)³⁰⁻³⁴ and our parallel interest in NHC-stabilized molecular catalysts,⁶¹⁻⁶⁶ we were interested in incorporating NHC ligands into the CCMs. Rhodium(I) complexes bearing NHC ligands have been successfully used for the hydrogenation of alkenes,⁶⁷⁻⁷⁶ although complexes bearing monodentate NHCs were prone to decomposition due to Rh-NHC bond cleavage.⁷²

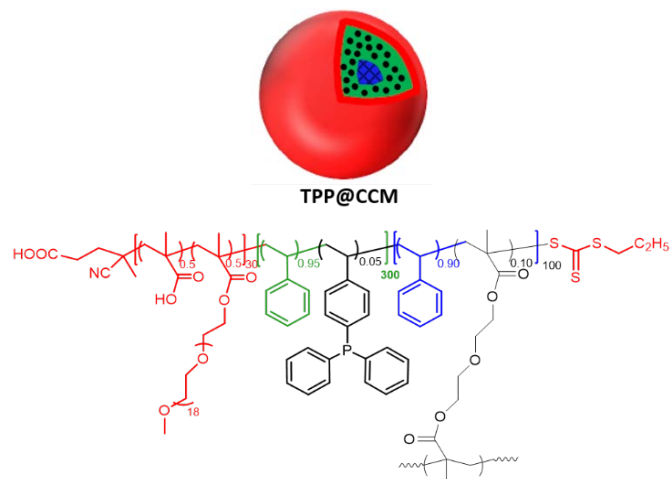


Figure 2. TPP@CCMs developed in our group.

We wondered whether the incorporation of simple monodentate NHC-Rh complexes into our polymer scaffold could allow their stabilization and prevent their decomposition under hydrogenation conditions.

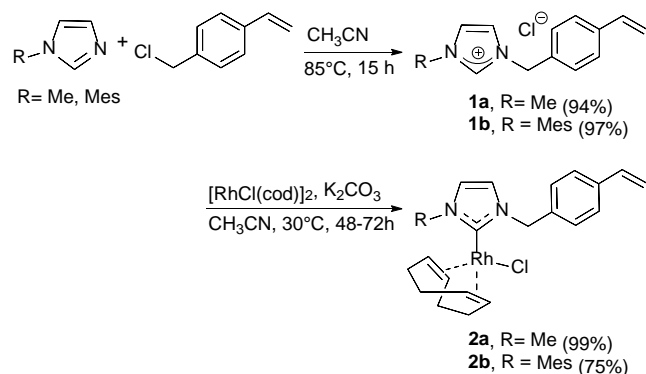
We thus describe here CCMs that incorporate rhodium(I) complexes bearing monodentate N-heterocyclic carbene ligands. The complexes have been covalently bound to the polymeric chains by incorporation of a polymerizable unit on the NHC ligand. Two different N substituents have been used in order to probe their influence on the CCM properties and activity in styrene hydrogenation under aqueous biphasic conditions.

Results and discussion

Synthesis and characterization of polymerizable Rh(I) complexes

Polymerizable imidazolium salts **1a-b**, precursors of NHC ligands, have been obtained in one step by the quaternization of either *N*-methylimidazole (**1a**) or *N*-mesitylimidazole (**1b**) with 4-vinylbenzyl chloride (Scheme 1). Both were obtained in excellent yields on a multi-gram scale. Analytical data of **1a** were consistent with those reported in the literature,⁷⁷ while imidazolium salt **1b** (reported only once with no available experimental details⁷⁸) was fully characterized. The synthesis of the rhodium(I) complexes was then carried out in the presence of [RhCl(COD)]₂ and K₂CO₃ as base in MeCN following a previously reported protocol.⁷⁹ These mild reaction conditions allowed us to obtain the expected polymerizable complexes **2a-**

b in good to excellent yields as air-stable, bright yellow powders.



Scheme 1. Synthesis of polymerizable rhodium(I) complexes **2a** (R = Me) and **2b** (R = Mes).

Both complexes were characterized by NMR and mass spectrometry. In the ^1H NMR spectra, the disappearance of the characteristic acidic proton of the imidazolium moiety at 10.4–10.5 ppm was observed as well as the shift of the two other heterocyclic protons. The presence of the vinylic protons was confirmed and the signals of the COD ligand became differentiated. The best proof of coordination of the NHC ligand is the doublet at 183.0 ppm ($J_{\text{RhC}} = 51.2$ Hz, **2a**) and 182.9 ppm ($J_{\text{RhC}} = 51.5$ Hz, **2b**) in the ^{13}C NMR spectrum. These chemical shifts and coupling constants are typical of the C2 carbon of an imidazol-2-ylidene moiety coordinated to rhodium(I).

Single crystals suitable for X-ray diffraction analyses were also obtained for both complexes by slow diffusion of pentane in a dichloromethane solution (Fig. 3). Both compounds crystallized in monoclinic form, in the $P2_1/c$ space group for **2a** and $P2_1/n$ space group for **2b**. The coordination geometry is square planar with bond lengths and angles within the ranges reported for similar neutral, monodentate NHC-Rh(I) complexes (Table 1).^{72, 80, 81} Methyl and mesityl substituents were chosen to evaluate the steric effect on the catalytic activity of the rhodium complexes. We also surmised that the presence of the aromatic mesityl substituent may help to solubilize the complex in lipophilic media.

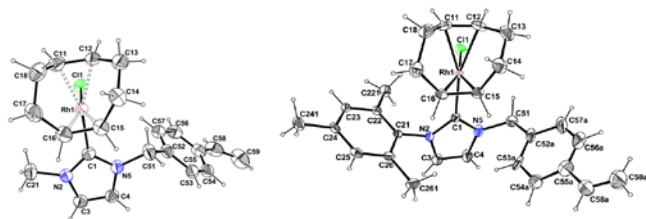


Figure 3. ORTEP representations of complexes **2a** (left) and **2b** (right). Ellipsoids are shown at the 30% level.

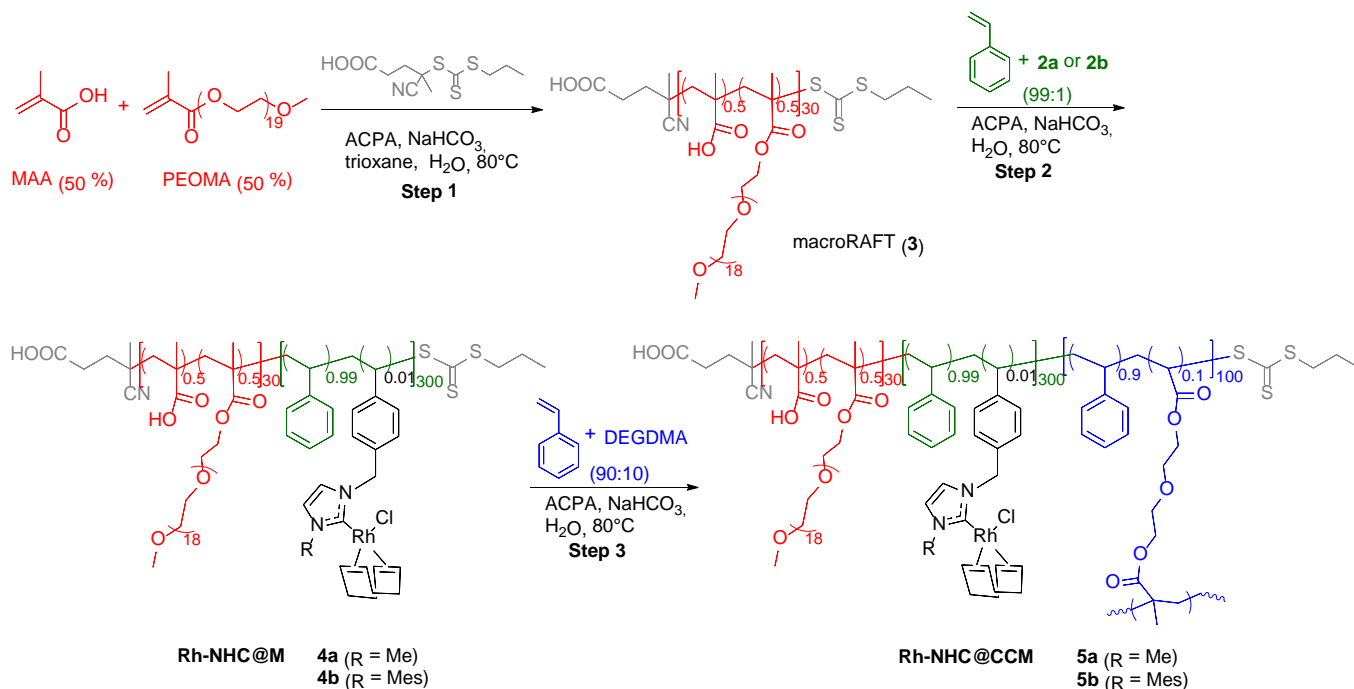
Table 1. Selected bond distances (Å) and angles (deg) of complexes **2a** and **2b**.

	2a	2b
Rh(1)-C(1)	2.030 (4)	2.034 (3)
Rh(1)-Cl(1)	2.3763	2.3839 (9)
	(10)	
N(2)-C(1)	1.353 (5)	1.359 (4)
N(5)-C(1)	1.350 (5)	1.351 (4)
C(3)=C(4)	1.336 (6)	1.328 (5)
C(1)-Rh(1)-Cl(1)	89.36 (10)	87.78 (10)
N(1)-C(1)-N(2)	104.3 (3)	103.7 (3)

Synthesis and characterization of Rh-NHC@CCMs

The Rh-containing CCMs, possessing a Rh-functionalized hydrophobic core and a hydrophilic shell, were synthesized by RAFT polymerization in water (Scheme 2), using the PISA approach (Polymerization Induced Self Assembly),⁸²⁻⁸⁵ as already applied earlier in our group for the synthesis of the phosphine-containing CCMs.^{30-32, 34, 35, 37} In the first step, the RAFT copolymerization of methacrylic acid (MAA) and poly(ethylene oxide) methacrylate methyl ether, $\text{CH}_2\text{CH}(\text{CH}_3)\text{COO}(\text{CH}_2\text{CH}_2\text{O})_{19}\text{Me}$ (PEOMA), in a 1:1 molar ratio in water using $\text{R}_0\text{-SC(S)SPr}$ (CTPPA, $\text{R}_0 = -\text{C}(\text{CH}_3)(\text{CN})\text{CH}_2\text{CH}_2\text{COOH}$) as RAFT agent generated a $\text{R}_0\text{-(MAA}_{15}\text{-co-PEOMA}_{15})\text{-SC(S)SPr}$ macromolecular RAFT agent (**3**, macroRAFT). The second step was in our case the most important one, since it consisted in the chain extension of the hydrophilic P(MMA-co-PEOMA) block with the hydrophobic one by the co-incorporation of styrene and the polymerizable rhodium(I) complex. Styrene (St) and **2a** or **2b** were added to generate $\text{R}_0\text{-(MAA}_{15}\text{-co-PEOMA}_{15})\text{-b-(St)}_{297}\text{-co-(2a/b)}_3\text{-SC(S)SPr}$ amphiphilic block copolymers (**4a** and **4b**) that self-assembled into nanometric micellar particles. This chain extension of macroRAFT **3** is closely related to others, which used mixtures of styrene and other ligand-functionalized styrenes (triphenylphosphine,³⁰ bis(*p*-methoxyphenyl)phenylphosphine,⁸⁶ nixantphos³⁶) and proceed with excellent control of the molar mass and low dispersity. Fractions of the rhodium monomer **2a** (Rh-NHC^{Me}) greater than 1% could not be used because of the rather low solubility of this monomer in styrene. In addition, polymer precipitation was observed instead of the formation of a stable colloidal dispersion when applying the classical reaction conditions, namely mixing all components including the radical initiator before heating. To overcome this problem, the macroRAFT agent was first mixed with the two comonomers (styrene + Rh complex) and stirred at 80°C for 30 min, before adding the ACPA/ NaHCO_3 initiating solution: a well-behaved copolymerization with the formation of a stable latex was observed in this case. The same procedure was successfully applied to the synthesis of micelles **4b**.

Finally, in the last step, addition of a cross-linker, namely diethylene glycol dimethacrylate (DEGDMA), allowed the generation of core-crosslinked particles (CCMs) **5a** and **5b** as beige, milky aqueous dispersions.



Scheme 2. Synthesis of the Rh-NHC^R@CCMs **5a** (R = Me) and **5b** (R = Mes) by RAFT-PISA polymerization.

The CCMs **5a** and **5b**, also named respectively Rh-NHC^{Me}@CCM and Rh-NHC^{Mes}@CCM, were analysed by dynamic light scattering (DLS) and transmission electron microscopy (TEM). The average size (D_z) and polydispersity index (PDI) of CCMs **5a** and **5b** from the DLS analyses are reported in Table 2.

Table 2. DLS analyses of nanoreactors **5a** and **5b**.

	D_z (nm)	PDI	Solid content (%)	[Rh] (mol·L ⁻¹)
5a	121	0.145	22.9	0.0115
5b	178	0.09	22.8	0.0094

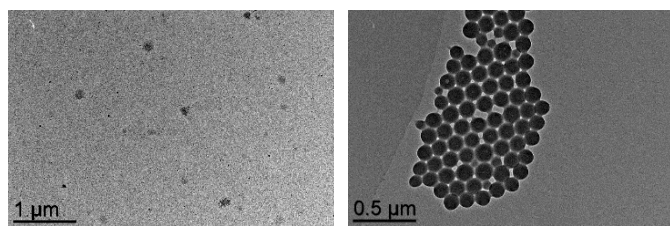


Figure 4. Morphology of nanoreactors: TEM images of Rh-NHC^{Me}@CCM **5a** (left) and Rh-NHC^{Mes}@CCM **5b** (right).

The **5b** particles are larger and with a narrow size distribution, indicative of good homogeneity. On the other hand, the **5a** sample shows a smaller average size and a greater size dispersity, but more particularly the presence of a shoulder in volume, which may suggest the existence of more than one population of particles (see S.I., DLS section).

In order to confirm the shape and dimensions of the CCMs, transmission electron microscopy was performed on both samples. Whereas the TEM images of **5b** reveal particles with a spherical shape, regular dimensions and a relatively narrow size distribution with an average diameter of 123.3 (\pm 19.2) nm (Figure 4 and S.I., TEM section), the images of **5a** display a

mixture of particles with a broad size distribution and non-spherical shape, which also leaves a doubt about the incorporation of the rhodium-containing monomer in the CCMs. After several months of storage, the **5a** latex showed partial precipitation and a darkened colour, whereas the latex of **5b** kept the same beige and homogeneous aspect. This led us to think that only complex **2b** was efficiently and homogeneously incorporated into the hydrophobic core of the CCMs.

NMR studies were carried out on latex **5b** to confirm the unchanged nature of the Rh complex, and more particularly the integrity of the Rh-carbene bond, upon polymerization. To verify the effective polymerization of rhodium complex **2b** and its incorporation into the hydrophobic core, a ¹³C-labeled analogue of the polymerizable rhodium(I) complex (**2b**^{*}) was prepared according to Scheme 1 from C2-labeled N-mesitylimidazole, and introduced into CCMs. In order to ensure complete incorporation of **2b**^{*} into the polymer network, heating was prolonged in step 2 (Scheme 2) and more ACPA was added after complete consumption of the first portion. **5b**^{*} was thus obtained as a beige latex. It was concentrated to a slurry that was swelled by addition of a few drops of THF-*d*₈, in order to get a gel with better local mobilities. The latex gel was analysed by magic angle spinning (MAS) ¹H and ¹³C NMR measurements (Figure 5) that yielded spectra of **5b**^{*} with narrow signals and good resolution. In the ¹³C-MAS spectrum, a distinctive doublet at 182.7 ppm ($J_{\text{RhC}} = 47$ Hz) could be observed and unambiguously attributed to the carbenic carbon coordinated to rhodium.

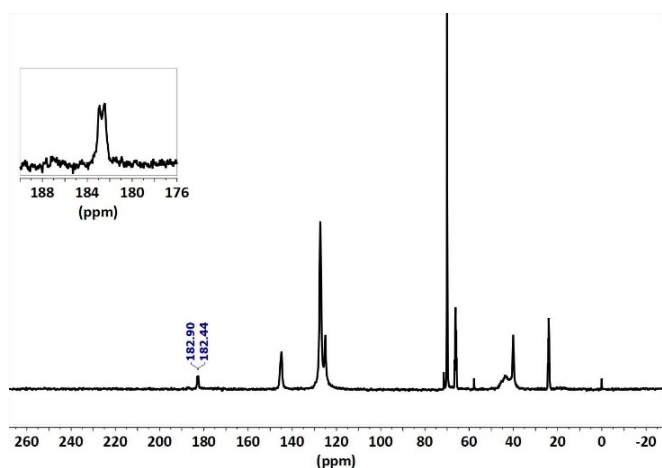


Figure 5. Solid-state ^{13}C -MAS NMR spectrum of ^{13}C -labeled Rh-NHC^{mes}@CCMs **5b*** ($\text{H}_2\text{O}/d_8$ -THF gel).

In addition, analysis of the dipolar filtered ^1H -DFSE-MAS NMR spectrum, that allows the edition of very mobile species (see S.I.),⁸⁷ confirmed the absence of residual monomer **2***: no signal was observed around 5.8 ppm, where a characteristic vinylic proton signal of monomer **2*** usually appears in THF- d_8 . No signals of the *N*-mesityl methyl groups, situated between 1.9 and 2.5 ppm, were observed either. We therefore assumed that the amount of residual monomer **2*** was below the NMR detection limit (< 1%) and that the signal observed at 182.7 ppm by ^{13}C NMR was solely due to core-polymerized rhodium(I) complex.

To assess the effect of catalyst incorporation into the nanoparticle **5b** on its catalytic activity, the model rhodium(I) complex **7b** bearing a methyl group in place of the vinyl group (Fig. 6), for use under “classical” homogeneous conditions, was prepared from the corresponding imidazolium salt **6b** according to the same procedure as complex **2b**. *N*-methyl-substituted analogues **6a** and **7a** were not prepared, as the incorporation of the polymerizable rhodium(I) complex **2a** into CCMs did not prove successful.

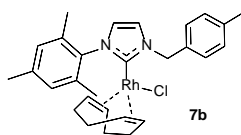


Figure 6. Model rhodium(I) complex **7b** used in this study.

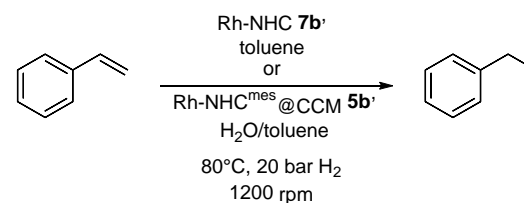
Rh-catalysed hydrogenation of styrene

As mentioned above, Rh(I) complexes bearing NHC ligands are active catalysts for the hydrogenation of alkenes. However, those bearing monodentate NHC ligands tend to decompose under H_2 .⁷⁰⁻⁷² This was first demonstrated by Herrmann and Frey in 2007⁷² in 1-octene hydrogenation investigations with several such complexes. In the absence of an additional ligand such as PPh_3 to complete the coordination sphere, the complexes decomposed to yield black Rh^0 as either rhodium particles or colloids. Even though the latter proved relatively active for hydrogenation, this diminished the interest of Rh(I)-

NHC complexes as hydrogenation catalysts. More recently, Bullock et al. studied the real nature of the active species in the hydrogenation of arenes in the presence of $[(\text{CAAC})\text{RhCl}(\text{COD})]$ and showed that Rh-CAAC nanoparticles are the active species also under their experimental conditions.⁸⁸

Our catalytic investigations have dealt with styrene hydrogenation under both homogeneous and aqueous biphasic conditions. The model rhodium complex **7b** was thus used for the hydrogenation of styrene under “classical” homogeneous conditions in toluene, whereas the activity of Rh-NHC^{mes}@CCM **5b** was evaluated in a biphasic water-toluene mixture (Table 3). Since the nanoreactor core is hydrophobic, it should in principle protect the catalyst from direct contact with the water phase, but the core penetration by small water amounts, according to the water solubility in toluene, cannot be excluded. Therefore, in order to better compare the catalyst performance under the homogeneous and biphasic conditions, different experiments were carried out with complex **7b**: in dry toluene (ca. 5 ppm of residual H_2O after drying, according to a Karl-Fischer titration), in “wet” toluene (i.e. toluene taken directly from the bottle without further drying, containing 180 ppm of H_2O) and “on-water” conditions with excess water added to the organic solution. In our opinion, the second experiment (i.e. in “wet” toluene) should best mimic the nanoreactors core environment.

Table 3. Rh-catalysed hydrogenation of styrene.



	Cat.	Solvent	Sty/Rh	t(h)	Styrene conv.(%) ^e
1	7b	Toluene (dry) ^a	1000/1	6	1
2	7b	Toluene (wet) ^b	1000/1	6	4
3	7b	Tol/ H_2O ^c	1000/1	3	19
4	“	“	“	6	95 ^f
5	5b	Tol/ H_2O ^c	1000/1	3	>99.5
6	“	“	“	6	>99.5
7	5b	Tol/ H_2O ^c	10 000/1	1	12
8	“	“	“	3	73
9	“	“	“	6	>99.5
10	7b	Tol/DME (1:1) ^d	1000/1	6	>99.5
11	7b	Tol/DME (1:1) ^d	10 000/1	3	39
12	7b	Tol/“blank” CCMs	1000/1	6	>99.5

Homogeneous conditions (entries 1-4 and 10-12): styrene (1.04 g, 10 mmol), rhodium complex **7b** (5.8 mg, 0.01 mmol; Sty/Rh:1000/1 or 0.6 mg, 0.001 mmol, Sty/Rh:10 000/1), decane (426 mg, 3 mmol), toluene (1mL) / water or DME (0.5 mL). Biphasic conditions (entries 5-9): styrene (79.3 mg, 0.75 mmol), CCM **5b** (85 mg, $7.9 \cdot 10^{-7}$ mol of Rh for Sty/Rh:1000/1 or 8.5 mg, $7.9 \cdot 10^{-8}$ mol of Rh for Sty/Rh:10 000/1), decane (31.5 mg, 0.225 mmol), toluene (1mL) / water (0.5 mL). ^a Dry toluene: 5 ppm H_2O (K.F.). ^b “Wet” toluene: no purification, from the bottle, 180 ppm H_2O (K.F.). ^c 0.5 mL of water (**7b**) or aqueous phase (**5b**). ^d DME (dimethoxyethane): 155 ppm H_2O (K.F.). ^e Measured by GC. ^f 90% selectivity in ethylbenzene, calculated by GC.

Initial reactions were carried out at 80°C under 20 bar of H₂, with a molar styrene/Rh ratio of 1000/1. Pleasingly, a total conversion of styrene to ethylbenzene was observed under these conditions with **5b** (entries 5 and 6), versus <5% conversion with molecular catalyst **7b** after 6 h in dry or “wet” toluene (entries 1 and 2). This reactivity difference was consistently reproduced. Using “on-water” conditions, however, complex **7b** surprisingly gave again a high hydrogenation activity (entry 4). After 3 h, the conversion with molecular catalyst **7b** was low (19%, entry 3), whereas a total conversion was already reached with CCMs **5b** (entry 5). However, both systems gave a quasi-quantitative conversion after 6 h (entries 4 and 6), albeit with an incomplete GC mass balance for the reaction under homogeneous conditions (9 mmoles total for 10 mmoles expected). Given the observed high efficiency of **5b**, the catalytic loading was reduced by a factor of 10 (entries 7-9). The conversion was low after 1 h (entry 7) at 80°C, but complete after 6 h (entry 9). After 3 h, it reached 73% (entry 8), which is much higher than that reached with molecular catalyst **7b** under “on-water” conditions (entry 3), in spite of the 10 times greater catalytic loading in the latter case. Visually, the mixture resulting from the “on-water” catalysis experiments (entries 3-4) presented a large amount of a black precipitate, characteristic of catalyst degradation, whereas the mixture resulting from the classical homogeneous conditions (entries 1-2) remained bright yellow, with only traces of black precipitate. This indicates that complex **7b** was efficiently activated in the presence of water, though with extensive reduction to metallic particles, which are apparently able to catalyse styrene hydrogenation with a greater activity than the molecular complex. This behaviour is consistent with Herrmann and Frey’s early observations of a black precipitate obtained in the absence of an additional stabilizing phosphine ligand.⁷² Our group also observed very recently the formation of Rh⁰ NPs from [RhCl(COD)(TPP@CCM)] latexes, when these are subjected to an H₂ pressure in the absence of olefins. These Rh⁰ NPs are highly active as catalysts for styrene hydrogenation.⁸⁹ As the CCM core is not only constituted of a polystyrene network but also contains a high number of poly(ethylene oxide) moieties in the shell (PEOMA), which can enter the cores of swollen nanoreactors,³⁵ it was envisaged that they may play a role in the activation and stabilisation of the rhodium catalytic species. Therefore, two additional reactions were carried out under homogeneous conditions with **7b** in a toluene/DME 1:1 mixture, in order to mimic the polyether environment of the CCMs. After 6h at a 1000/1 styrene/Rh ratio (entry 10), the mixture remained mostly yellow, with only traces of black precipitate, but surprisingly the conversion into ethylbenzene was total, in stark contrast with the reactivity observed in pure toluene (entry 2). This is a good indication that the polyether chains play an active role in the activation/stabilisation of the catalyst within the CCMs, without contributing to the formation of Rh nanoparticles. Then a 10 000/1 styrene/Rh ratio was set and the reaction was stopped after 3h (entry 11). In this case, the conversion was only 39%, versus 73% with **5b** under aqueous biphasic conditions (entry 8). This seems to indicate that the confinement effect of the CCM also contributes to the activity boost. We imagine that the

presence of water, on the contrary, may facilitate the formation of metal nanoparticles, which is a commonly observed phenomenon also for palladium catalysts bearing NHC ligands.⁹⁰ Conversely, no black precipitate was observed at the end of the reaction with the nanocatalysts, which is consistent with the catalyst confinement within the CCM hydrophobic environment, from which water as a bulk phase is excluded. Thus, water cannot exert its action to promote the metal reduction and the observed behaviour may correspond to that observed for the molecular complex under homogeneous conditions, except for the much greater catalytic activity. In any case, the possible formation of Rh nanoparticles cannot account for the immediately high catalytic activity in the first run, which must therefore be attributed to a molecular Rh^I complex. The ethylbenzene selectivity was total in all cases.

Covalent bonding of the Rh complex in the CCM core proved necessary for an efficient handling and recycling of the nanocatalysts. When the model Rh complex **7b** was added as a toluene solution to the aqueous phase of “blank” CCMs (*i.e.* possessing a non-functionalized polystyrene core), complete conversion of styrene to ethylbenzene was obtained under optimized conditions (6 h, 80 °C, 1000/1 styrene/Rh, entry 11) and an important amount of Rh⁰ particles was produced after only one run and made the phase separation difficult (see photos in the S.I.). Moreover, it is impossible to tell whether styrene reacted with the catalyst that penetrated in the core with the swelling solvent, or with the catalyst still present in the organic phase.

Recycling of the aqueous phase of **5b** was investigated on 3-hour runs at 80°C (Table 4). After reaction, decantation, organic phase removal and further extraction of the aqueous phase with toluene, a new portion of styrene in toluene was added to the recovered latex. It was thus possible to recycle **5b** four times, maintaining full styrene conversion and ethylbenzene selectivity, under the optimized conditions (3 h at 80°C with a 1000/1 styrene/Rh ratio, entries 1-5).[‡] Photos of the aqueous phases recovered after runs 1 and 5, respectively (see S.I.), suggest a possible slow formation of Rh⁰.

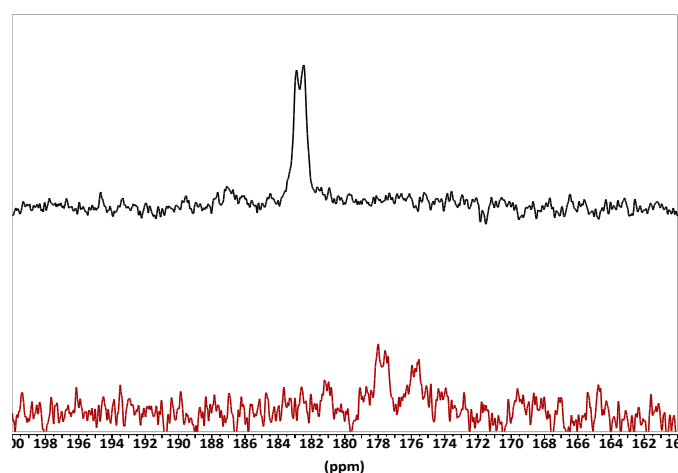
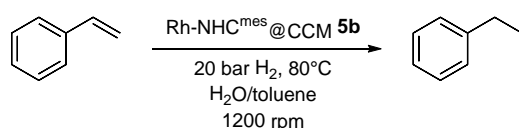


Figure 7. solid-state ¹³C-MAS NMR spectra of ¹³C-labelled **5b*** before catalysis (black) and after 5 hydrogenation runs (red).

The aqueous phase recovered after 5 runs was analysed by solid-state ¹³C-MAS NMR, which distinctively showed two

doublets at, respectively, 177.8 ($J_{\text{RhC}} = 43$ Hz) and 175.8 ppm ($J_{\text{RhC}} = 42$ Hz) (Figure 7 and S.I.). While the exact nature of these species could not be determined, the signals multiplicity and value of coupling constants prove that NHC-Rh(I) species are still present in the CCMs. The shift from the initial 182.7 ppm value (Fig. 7) may be explained by the hydrogenation of COD, necessary for the activation of the complex, and its replacement by a molecule of solvent or substrate from the reaction medium. As suggested from the photos, TEM images of the same aqueous phase revealed the presence of small-size objects, likely corresponding to Rh^0 nanoparticles, within the CCMs (see S.I., TEM section). Although their small number did not allow for an accurate size distribution measurement, diameters between 2.1 and 2.7 nm were observed. However, it was difficult at this point to conclude on the role of these NPs on the catalytic activity and to check by ^{13}C -MAS NMR whether the NHC ligand was bound to their surface (a strong Knight shift,⁹¹ in the case of Rh NPs, could prevent the observation of the ^{13}C NMR signal of surface-bound NHCs). From the data collected by NMR and TEM, the coexistence of Rh^I and Rh⁰ species in the nanoreactors seems the most likely situation.

Table 4. Rh-catalysed hydrogenation of styrene: recycling experiments with Rh-NHC^{mes}@CCM **5b** ($\text{H}_2\text{O}/\text{toluene}$, 20 bar H_2 , 80°C, 3h).



Run	Sty/Rh	Styrene conv. (%) ^a	EtBz selectiv. (%) ^a	Rh leaching (ppm) ^b	
1	1 st	1000/1	>99.5	>99.5	0.87
2	2 nd	"	>99.5	>99.5	1.47
3	3 rd	"	>99.5	>99.5	0.24
4	4 th	"	>99.5	>99.5	0.34
5	5 th	"	>99.5	>99.5	0.21
6	1 st	10 000/1	73	>99.5	0.39
7	2 nd	"	77	>99.5	0.61
8	3 rd	"	>99.5	>99.5	0.54
9	4 th	"	>99.5	>99.5	0.31
10	5 th	"	98	>99.5	0.13

Conditions: styrene (79.3 mg, 0.75 mmol), CCM **5b** (85 mg, $7.9 \cdot 10^{-7}$ mol of Rh for Sty/Rh:1000/1 or 8.5 mg, $7.9 \cdot 10^{-8}$ mol of Rh for Sty/Rh:10 000/1), decane (31.5 mg, 0.225 mmol), toluene (1mL) / water (0.5 mL).^a Measured by GC. ^b Measured by ICP-MS.

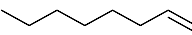
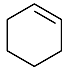
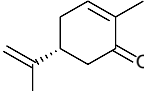
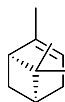

Four three-hour recycle runs were also carried out with the lower catalytic loading, i.e. with an initially incomplete styrene conversion (entries 6-10). Interestingly, the styrene conversion was complete after the third run (entry 8), and thus higher than after the initial run (entry 6). This indicates the presence of a pre-catalyst activation phase during the first runs, presumably involving the hydrogenation of the COD ligand. Only after the

4th recycle was a slight loss of activity detected, with a styrene conversion of 98% (entry 10). This could be explained by gradual Rh^0 nanoparticles formation, which have a propensity to migrate and accumulate outside the core, as seen from the TEM images of **5b***, and as demonstrated in our recent investigation of the Rh^0 NPs obtained from $[\text{RhCl}(\text{COD})(\text{TPP}@CCM)]$ latexes:⁸⁹ they can agglomerate in the PEO-containing shell of the CCMs and thus lose active surface, leading to a diminished catalytic efficiency.

The rhodium leaching per cycle was then measured by ICP-MS on each 3h-reaction set. Pleasingly, the loss of rhodium per cycle was on average inferior to 0.6 ppm, except for the first two runs at a 1000/1 styrene/Rh ratio (entries 1 and 2), where a maximum value of ca. 1.5 ppm was measured. These values are consistent with what has been observed in the case of phosphine-containing TPP@CCMs, also used as nanocatalysts for the biphasic hydrogenation of styrene and 1-octene.³³ The latter possess the same outer shell with poly(ethylene oxide) chains. The loss of rhodium into the organic phase is probably not due to decomposition of the rhodium complex by cleavage of the ligand-metal bond, as shown by the solid-state ^{13}C -MAS NMR spectrum of CCMs after 5 runs. Moreover, the CCMs are still active after 5 cycles with no loss of selectivity. This small amount of leaching has generally been attributed to the polymer architecture (mass transport, lipophilicity at higher temperatures).^{30, 31, 34} In the case of a 10 000/1 styrene/Rh ratio, the cumulated rhodium loss over 5 cycles (1.98 ppm) was evaluated at 24% of the molar amount of Rh present in the core of the CCMs, which can explain a slight drop in activity after 5 runs. On the other hand, this loss (3.13 ppm) was only 4% of the total amount of Rh in the case of a 1000/1 styrene/Rh ratio. The DLS analyses of the recycled aqueous phase after each run, for the 3 h experiments with a 10 000/1 styrene/Rh ratio, showed an invariance of the average size and size distribution, demonstrating the stability of the polymer scaffold (see S.I., DLS section).

As CCMs **5b** showed a high efficiency for styrene hydrogenation, we extended their use to other alkene substrates (Table 5). Thus, hydrogenation of 1-octene and cyclohexene was investigated under aqueous biphasic conditions with **5b** (10 000/1 substrate/Rh ratio). 1-octene was almost completely consumed, but the reaction proved poorly selective, with 65:35 octane/2-octenes (entry 1). It is well-known that 1-octene can isomerize more easily into 2-octenes in the presence of NHC-stabilized Rh(I) complexes compared to their phosphine analogues,^{72, 92} but these results suggest that the nature of the environment may also influence the selectivity. Cyclohexene was hydrogenated to cyclohexane with 68% conversion (entry 2) and a low 60% selectivity (incomplete GC mass balance). Hydrogenation of monoterpenes such as carvone, α - and β -pinene did not prove successful: with (*R*)-(-)-carvone (entry 3), only traces of product having the *exo* double bond hydrogenated were observed by GC-MS. Finally, with **5b**, no reaction occurred in the case of (1*R*)-(+)- α -pinene (entry 4), whereas reaction with (1*S*)-(-)- β -pinene gave 13% isomerization to α -pinene and less than 5% of the expected pinanes (entry 5).

Table 5. Substrate scope for Rh-catalysed hydrogenation with Rh-NHC^{mes}@CCM **5b** (10 000/1 substrate/Rh ratio, H₂O/toluene, 80°C, 20 bar H₂, 6h, 1200 rpm).

	Substrate	Conv. (%) ^a	Selectiv. (%) ^a
1		98	65
2		68	60
3		n.r.	-
4		n.r.	-
5		17	<30

^a Measured by GC.

Several hypotheses could explain the much greater activity of the polymer-anchored molecular catalyst with styrene: the polymer network, mostly constituted of polystyrene and ethylene oxide chains in the core, probably stabilizes coordinatively unsaturated intermediates of the catalytic cycle, whereas the homogeneous complex may be deactivated by bimolecular pathways, generating less active (or inactive) aggregated forms.

Moreover, the reduction to Rh⁰ occurs rapidly only in the presence of water, which is present in very small amounts in the core. In addition, the free diffusion of the rhodium atoms in **5b** is restricted by the polymer anchoring, slowing down the nanoparticle formation relative to the homogeneous phase. Note that the concentration factor alone should favour faster aggregation in the polymer: the Rh-functionalized monomers (1% mol) in the polystyrene yield an approximate Rh concentration of 0.1 M in the polymer core, vs. a 10 times smaller value in the homogeneous solution. Finally, a higher local concentration of substrate is expected due to confinement in the core, leading to a higher reaction rate in the case of CCMs.

Conclusions

In summary, we have prepared a well-defined polymeric nanoreactor containing a Rh(I)-NHC complex in the hydrophobic core by a RAFT-PISA copolymerization procedure in water. For this purpose, polymerizable Rh complexes with styrene-functionalized NHC ligands (**2a** and **2b**) have been prepared and fully characterized. They are air-stable and can be stored for months without any sign of decomposition, making them potentially useful for incorporation in a wider variety of nanostructures. The air-stable nanoreactor **5b**, called Rh-NHC^{mes}@CCM, which is maintained in stable aqueous dispersions (latex), has been characterized by NMR, DLS and TEM and evaluated as catalyst for the aqueous biphasic hydrogenation of styrene and other alkenes. It has a greater activity and its evolution to Rh⁰ is slower relative to its

analogous molecular Rh(I) complex for the hydrogenation of styrene. Finally, the **5b** latex could be recycled up to four times with almost no loss of activity over 3 h cycles. The confined nature of the CCM core, as well as stabilization of the intermediate catalytic species by the hydrophobic polymer network, may be responsible for this marked gain of reactivity in the case of styrene. Research is in progress to optimize the synthesis of the Rh-NHC@CCMs and to extend this strategy to other catalytic systems.

Experimental section

General

All manipulations were performed under an inert atmosphere of dry argon by using Schlenk line techniques. Solvents were either dried by standard procedures and distilled under argon prior to use, or purified on an Innovative PURESOLV Solvent Purification System equipped with 4Å MS columns. All reagents, unless stated otherwise, were used as received. ¹³C-labelled formaldehyde (98%, ca. 20% w/w in H₂O) was purchased from Eurisotop and used as received. Dihydrogen was obtained from Air Liquide (AlphagazTM 1 with purity ≥99.999%). Styrene (99%, Acros) was purified by passing through a column of active basic aluminium oxide to remove the stabilizer. The RAFT agent 4-cyano-4-thiothiopropylsulfanyl pentanoic acid (CTPPA)⁹³, macroRAFT agent **3**³⁰ and 1-methyl-3-(4-vinylbenzyl)imidazolium chloride **1a**⁷⁷ were synthesized according to published procedures.

Characterization techniques

NMR. ¹H NMR and ¹³C NMR spectra were recorded in 5 mm diameter tubes at 298 K in CDCl₃, D₂O, DMSO-*d*₆ or THF-*d*₈ using Bruker Avance III 400 spectrometer. Magic Angle Spinning (MAS) NMR experiments were performed on a Bruker Avance 400 III HD spectrometer with the sample insert into a 4 mm zirconia rotor. The rotors were spun at 6 kHz at 298 K. ¹H MAS with rotor synchronous dipolar filtering and spin echo excitation (DFSE)⁸⁷ were acquired with a filtering time of 800 ms. ¹³C MAS was done with a recycle delay of 5 s. The chemical shifts were determined relative to tetramethylsilane using the deuterated solvent as internal standard for liquid state NMR or an external solution for solid state NMR. For the CCMs synthesis, 1,3,5-trioxane (δ 5.20 in the ¹H NMR in D₂O) was used as an integration reference.

Electrospray (ES) mass spectroscopy. Mass spectra were recorded at the Université Paul Sabatier by the Service Commun de Spectrométrie de Masse on a MS/MS Q TRAP 2000 (Applied Biosystems) or API-365 (Perkin Elmer Sciex).

X-ray structural analyses. A single crystal of compound **2a** was mounted under inert perfluoropolyether at the tip of a glass fibre and cooled in the cryostream of a Rigaku Oxford Diffraction GEMINI EOS equipped with Mo-Kα radiation, whereas a single crystal of compound **2b** was mounted on a Bruker Apex2 equipped with Mo-Kα radiation using a micro source. The structures were solved by the Integrated Space-Group method using the SHELXT software⁹⁴ and refined by least-

squares procedures on F^2 using SHELXL-2015.⁹⁵ All H atoms attached to carbon were introduced in the calculation in idealized positions and treated as riding models. The drawing of the molecules was realized with the help of ORTEP32.⁹⁶ Crystal data and refinement parameters are shown in the S.I. CCDC deposition numbers for **2a** and **2b**: 2062972-2062973.

DLS (Dynamic Light Scattering). The intensity-average diameters of the latex particles (D_z) and the polydispersity index (PDI) were measured at 25°C on a Malvern Zetasizer NanoZS equipped with a He-Ne laser ($\lambda=633$ nm). After filtration through a 0.45 μm pore size membrane, deionized water was used to dilute the latex sample. Solutions were analysed without further filtration to ensure that undesired populations were not removed. Data were analysed by the general-purpose non-negative least squares (NNLS) method. The typical accuracy for these measurements was 10–15%.

TEM (Transmission Electron Microscopy). The morphological analyses of the copolymer nanoparticles were performed with a JEOL JEM 1011 transmission electron microscope equipped with 100 kV voltage acceleration and tungsten filament (Service Commun de Microscopie Electronique TEMSCAN, Centre de Microcaractérisation Raimond Castaing, Toulouse, France). Diluted latex samples were dropped on a formvar/carbon-coated copper grid and dried under vacuum.

Gas Chromatography/FID. At the end of the hydrogenation tests, the amounts of reactant and products in the organic phase were measured using a Shimadzu GC-2014 chromatograph equipped with a flame ionization detector (FID) and using helium as carrier gas. Separations were performed on a SLB-5ms capillary column (30 m*0.32 mm; 0.25 μm film thickness). An internal calibration method was used by adding a precise quantity of decane (99%, Sigma Aldrich) to the organic phase prior to hydrogenation. The response factors were determined by analysis of standard solutions of styrene and ethylbenzene.

ICP/MS. High resolution ICP/MS was used to quantify the rhodium catalyst leaching in the organic phase. The recovered organic phase was diluted with ultrapure water using a 10^5 volumetric dilution factor, high enough to ensure complete dissolution. In practice, a 100 mL volumetric flask was filled at $\sim 2/3$ with milli-Q water, then 10 μL of the organic phase were introduced using a micropipette. The flask was introduced into an ultrasound bath for 15 min. The solution was checked for complete dissolution of the organic component and the dilution was then completed with milli-Q water to the 100 mL mark and put into the ultrasound bath for an additional 45 min. To eliminate matrix effects, rhodium standards were prepared in the same way by starting with solutions of $[\text{RhCl}(\text{COD})]_2$ in toluene at various weight fractions of Rh, in the $(0.01-0.2)\cdot 10^{-9}$ range (10-200 ppt). The resulting aqueous phase was analysed on a Thermo Scientific Element XR instrument.

Synthetic procedures

1-(2,4,6-trimethylphenyl)-3-(4-vinylbenzyl)imidazolium

chloride 1b. To a solution of 4-vinylbenzyl chloride (2.50 g, 16.4 mmol, 2 eq) in dry acetonitrile (50 mL) was added 1-mesitylimidazole (1.48 g, 7.94 mmol, 1 eq). The reaction

mixture was heated at 85 °C for 24h, concentrated *in vacuo* and the residue was washed with Et_2O (3*50 mL). After drying under vacuum, the product was obtained as a beige oil (2.62 g, 97% yield). ^1H NMR (400 MHz, CDCl_3): δ (ppm) 10.43 (s, 1H, NCHN), 7.94 (s, 1H, NCH=CH), 7.47 (d, $J_{\text{HH}}=8.0$ Hz, 2H, arom. CH), 7.17 (d, $J_{\text{HH}}=7.9$ Hz, 2H arom. CH), 7.05 (s, 1H, NCH=CH), 6.75 (s, 2H, CH Mes), 6.47 (dd, $J_{\text{HH}}=17.6$ Hz, 10.9 Hz, 1H, CH=CH₂), 5.68 (s, 2H, NCH₂Sty), 5.54 (d, $J_{\text{HH}}=17.6$ Hz, 1H, CH=CH₂), 5.08 (d, $J_{\text{HH}}=10.9$ Hz, 1H, CH=CH₂), 2.11 (s, 3H, *p*-CH₃ Mes), 1.82 (s, 6H, *o*-CH₃ Mes). ^{13}C NMR (400 MHz, CDCl_3): δ (ppm) 140.8 (C_q), 138.2 (C_q), 137.6 (NCHN or CH=CH₂), 135.8 (NCHN or CH=CH₂), 134.0 (C_q), 133.3 (C_q), 130.7 (C_q), 129.6 (CH Mes or arom. CH), 129.3 (CH Mes or arom. CH), 126.8 (CH Mes or arom. CH), 123.4 (NCH=CH), 123.3 (NCH=CH), 114.9 (CH=CH₂), 52.6 (NCH₂Sty), 20.9 (*p*-CH₃ Mes), 17.4 (*o*-CH₃ Mes). MS (ES+) m/z 303 [M]⁺ (100). HRMS (ES+) calcd for C₂₁H₂₃N₂ 303.1861; found 303.1866.

Polymerizable rhodium(I) complex 2a. The imidazolium salt 1a (95.3 mg, 0.406 mmol, 1 eq), $[\text{Rh}(\text{COD})\text{Cl}]_2$ (100.0 mg, 0.203 mmol, 0.5 eq) and K₂CO₃ (67.2 mg, 0.487 mmol, 1.2 eq) were placed in a dry Schlenk under argon, and dry acetonitrile (15 mL) was added. The mixture was heated at 30°C for 48 h, then filtered through Celite and evaporated to dryness. The residue was purified by column chromatography on silicagel (eluent: CH₂Cl₂ then CH₂Cl₂/MeOH: 98/2) to give a yellow solid (179 mg, 99% yield). ^1H NMR (400 MHz, CDCl_3): δ (ppm) 7.39 (d, $J_{\text{HH}}=8.3$ Hz, 2H, arom. CH), 7.32 (d, $J_{\text{HH}}=8.3$ Hz, 2H, arom. CH), 6.81 (d, $J_{\text{HH}}=1.9$ Hz, 1H, NCH=CH), 6.69 (dd, $J_{\text{HH}}=17.6$ Hz, 10.9 Hz, 1H, CH=CH₂), 6.63 (d, $J_{\text{HH}}=1.9$ Hz, 1H, NCH=CH), 5.85 (d, $J_{\text{HH}}=14.8$ Hz, 1H, NCH₂Sty), 5.73 (dd, $J_{\text{HH}}=17.6$ Hz, 0.9 Hz, 1H, CH=CH₂), 5.66 (d, $J_{\text{HH}}=14.9$ Hz, 1H, NCH₂Sty), 5.24 ($J_{\text{HH}}=10.9$ Hz, 0.8 Hz, 1H, CH=CH₂), 5.04-5.02 (m, 2H, CH COD), 4.09 (s, 3H, NCH₃), 3.39-3.35 (m, 1H, CH COD), 3.26-3.23 (m, 1H, CH COD), 2.50-2.19 (m, 4H, CH₂ COD), 1.99-1.80 (m, 4H, CH₂ COD). ^{13}C NMR (400 MHz, CDCl_3): δ (ppm) 183.0 (d, $J_{\text{RhC}}=51.2$ Hz, C_q, NCN), 137.4 (C_q), 136.2 (CH=CH₂), 136.0 (C_q), 128.4 (arom. CH), 126.7 (arom. CH), 122.4 (NCH=CH), 120.4 (NCH=CH), 114.3 (CH=CH₂), 98.8 (d, $J_{\text{RhC}}=6.9$ Hz, CH COD), 98.6 (d, $J_{\text{RhC}}=7.0$ Hz, CH COD), 68.2 (d, $J_{\text{RhC}}=14.5$ Hz, CH COD), 68.0 (d, $J_{\text{RhC}}=14.5$ Hz, CH COD), 54.2 (NCH₂Sty), 37.8 (NCH₃), 33.2 (CH₂ COD), 32.6 (CH₂ COD), 29.0 (CH₂ COD), 28.7 (CH₂ COD). MS (ES+) m/z 409 [M-Cl]⁺ (100), 327 (50), 436 (40), 607 (20), 762 (15), 844 (15). HRMS (ESI): calculated for C₂₁H₂₆N₂Rh [M-Cl]⁺: $m/z=409.1151$, found $m/z=409.1150$.

Polymerizable rhodium(I) complex 2b. The imidazolium salt 1b (275.2 mg, 0.812 mmol, 1 eq), $[\text{Rh}(\text{COD})\text{Cl}]_2$ (200.0 mg, 0.203 mmol, 0.5 eq) and K₂CO₃ (134.4 mg, 0.974 mmol, 1.2 eq) were placed in a dry Schlenk under argon, and dry acetonitrile (30 mL) was added. The mixture was heated at 30°C for 48 h, then filtered through Celite and evaporated to dryness. The residue was purified by column chromatography on silicagel (eluent: CH₂Cl₂ then CH₂Cl₂/MeOH: 98/2) to give a yellow solid (300 mg, 67% yield). ^1H NMR (400 MHz, CDCl_3): δ (ppm) 7.47 (d, $J_{\text{HH}}=8.2$ Hz, 2H, arom. CH), 7.38 (d, $J_{\text{HH}}=8.2$ Hz, 2H, arom. CH), 7.13 (s, 1H, CH Mes), 6.95 (s, 1H, CH Mes), 6.93 (d, $J_{\text{HH}}=1.9$ Hz, 1H, NCH=CH), 6.78 (d, $J_{\text{HH}}=1.9$ Hz, 1H, NCH=CH), 6.75 (dd, $J_{\text{HH}}=17.6$ Hz, 10.9 Hz, 1H, CH=CH₂), 6.48 (d, $J_{\text{HH}}=15.3$ Hz, 1H, NCH₂Sty), 5.79 (dd, $J_{\text{HH}}=17.6$ Hz, 0.9 Hz, 1H, CH=CH₂), 5.60 (d, $J_{\text{HH}}=15.3$ Hz,

1H, NCH₂Sty), 5.30 (dd, $J_{\text{HH}} = 10.9$ Hz, 0.8 Hz, 1H, CH=CH₂), 4.93-4.90 (m, 1H, CH COD), 4.85-4.80 (m, 1H, CH COD), 3.37-3.32 (m, 1H, CH COD), 3.03-2.98 (m, 1H, CH COD), 2.49 (s, 3H, CH₃ Mes), 2.41 (s, 3H, CH₃ Mes), 2.17-1.97 (m, 3H, CH₂ COD), 1.88 (s, 3H, CH₃ Mes), 1.81-1.45 (m, 5H, CH₂ COD). ¹³C NMR (400 MHz, CDCl₃): δ (ppm) 182.9 (d, $J_{\text{RhC}} = 51.5$ Hz, C_q NCN), 138.7 (C_q), 137.3 (C_q), 137.2 (C_q), 136.8 (C_q), 136.3 (CH=CH₂), 136.1 (C_q), 134.3 (C_q), 129.6 (CH Mes), 128.2 (arom. CH), 128.1 (CH Mes), 126.7 (arom. CH), 123.4 (NCH=CH), 121.1 (NCH=CH), 114.3 (CH=CH₂), 97.3 (d, $J_{\text{RhC}} = 7.3$ Hz, CH COD), 97.2 (d, $J_{\text{RhC}} = 7.1$ Hz, CH COD), 68.7 (d, $J_{\text{RhC}} = 14.5$ Hz, CH COD), 67.5 (d, $J_{\text{RhC}} = 14.3$ Hz, CH COD), 55.2 (NCH₂Sty), 33.8 (CH₂ COD), 31.6 (CH₂ COD), 29.1 (CH₂ COD), 28.0 (CH₂ COD), 21.1 (CH₃ Mes), 19.8 (CH₃ Mes), 17.8 (CH₃ Mes). MS (ES+) m/z 513 [M-Cl]⁺ (100), 540 (27), 431 (12). HRMS (ESI): calculated for C₂₉H₃₄N₂Rh [M-Cl]⁺: $m/z = 513.1777$, found: $m/z = 513.1772$.

1-(2,4,6-trimethylphenyl)-3-(4-methylbenzyl)imidazolium

chloride 6b. To a solution of 4-methylbenzyl chloride (1.0 g, 7.11 mmol, 1.7 eq) in dry acetonitrile (15 mL) was added 1-mesitylimidazole (0.795 g, 4.27 mmol, 1 eq). The reaction mixture was heated at 85 °C for 24 h, concentrated *in vacuo* and the residue was washed with Et₂O (3*50 mL). After drying under vacuum, the product was obtained as a beige oil (1.01 g, 72% yield). ¹H NMR (400 MHz, CDCl₃): δ (ppm) 10.90 (s, 1H, NCHN), 7.53 (s, 1H, NCH=CH), 7.47 (d, $J_{\text{HH}} = 7.8$ Hz, 2H, arom. CH), 7.22 (d, $J_{\text{HH}} = 7.6$ Hz, 2H arom. CH), 7.09 (s, 1H, NCH=CH), 7.00 (s, 2H, CH Mes), 5.92 (s, 2H, NCH₂*p*-Tol), 2.37 (s, 3H, *p*-CH₃ Mes or *p*-CH₃ tol), 2.34 (s, 3H, *p*-CH₃ Mes or *p*-CH₃ tol), 2.07 (s, 6H, *o*-CH₃ Mes). ¹³C NMR (400 MHz, CDCl₃): δ (ppm) 141.2 (C_q), 139.4 (C_q), 138.7 (NCHN or 2xC_q), 134.2 (NCHN or 2xC_q), 130.8 (C_q), 130.6 (C_q), 130.1 (CH Mes or arom. CH), 129.8 (CH Mes or arom. CH), 129.1 (CH Mes or arom. CH), 123.1 (NCH=CH), 122.4 (NCH=CH), 53.5 (NCH₂*p*-Tol), 21.2 (*p*-CH₃ Mes or *p*-CH₃ tol), 21.1 (*p*-CH₃ Mes or *p*-CH₃ tol), 17.7 (*o*-CH₃ Mes). MS (ES+) m/z 291 [M]⁺ (100). HRMS (ES+) calcd for C₂₀H₂₃N₂ 291.1861; found 291.1869.

Model rhodium(I) complex 7b. The imidazolium salt **6b** (100 mg, 0.31 mmol, 1 eq), [Rh(COD)Cl]₂ (75.4 mg, 0.15 mmol, 0.5 eq) and K₂CO₃ (50.7 mg, 0.37 mmol, 1.2 eq) were placed in a dry Schlenk under argon, and dry acetonitrile (8 mL) was added. The mixture was heated at 30 °C for 48 h, then filtered through Celite and evaporated to dryness. The residue was purified by column chromatography on silicagel (eluent: CH₂Cl₂ then CH₂Cl₂/MeOH: 95/5) to give a yellow solid (158 mg, 96% yield). ¹H NMR (400 MHz, CDCl₃): δ (ppm) 7.31 (d, $J_{\text{HH}} = 8.0$ Hz, 2H, arom. CH), 7.23 (d, $J_{\text{HH}} = 7.8$ Hz, 2H, arom. CH), 7.13 (br s, 1H, CH Mes), 6.94 (br s, 1H, CH Mes), 6.90 (d, $J_{\text{HH}} = 1.9$ Hz, 1H, NCH=CH), 6.76 (d, $J_{\text{HH}} = 1.9$ Hz, 1H, NCH=CH), 6.45 (d, $J_{\text{HH}} = 15.1$ Hz, 1H, NCH₂*p*-Tol), 5.56 (d, $J_{\text{HH}} = 15.1$ Hz, 1H, NCH₂*p*-Tol), 4.93-4.88 (m, 1H, CH COD), 4.85-4.80 (m, 1H, CH COD), 3.39-3.34 (m, 1H, CH COD), 3.03-2.98 (m, 1H, CH COD), 2.49 (s, 3H, CH₃ Mes), 2.41 (s, 3H, CH₃ *p*-Tol or Mes), 2.39 (s, 3H, CH₃ *p*-Tol or Mes), 2.18-1.97 (m, 3H, CH₂ COD), 1.87 (s, 3H, CH₃ Mes), 1.80-1.46 (m, 5H, CH₂ COD). ¹³C NMR (400 MHz, CDCl₃): δ (ppm) 182.7 (d, $J_{\text{RhC}} = 51.5$ Hz, C_q NCN), 138.7 (C_q), 137.7 (C_q), 137.2 (C_q), 136.2 (C_q), 134.3 (C_q), 134.2 (C_q), 129.6 (arom. CH), 129.5 (CH Mes), 128.1 (arom. CH), 128.0 (CH Mes), 123.2 (NCH=CH), 121.0 (NCH=CH), 97.2 (d, $J_{\text{RhC}} = 7.4$ Hz, CH COD), 97.1 (d, $J_{\text{RhC}} = 7.1$ Hz, CH COD), 68.6 (d, $J_{\text{RhC}} = 14.5$ Hz, CH COD), 67.4 (d, $J_{\text{RhC}} = 14.5$ Hz, CH COD), 55.2 (NCH₂*p*-Tol),

33.8 (CH₂ COD), 31.6 (CH₂ COD), 29.1 (CH₂ COD), 28.0 (CH₂ COD), 21.2 (CH₃ *p*-Tol or Mes), 21.1 (CH₃ *p*-Tol or Mes), 19.8 (CH₃ Mes), 17.8 (CH₃ Mes). MS (ES+) m/z 501 [M-Cl]⁺ (100), 528 [M-Cl+27]⁺ (10). HRMS (ES+) calcd for C₂₈H₃₄N₂Rh [M-Cl]⁺ 501.1777; found 501.1781.

Synthesis of Rh-NHC@CCMs **5a** and **5b**

Step 1: the macroRAFT **3** was prepared according to our previously reported procedure.³⁰

Step 2: Chain extension of 3 by RAFT copolymerization of styrene and rhodium complex 2a or 2b in water: synthesis of 4a and 4b. 4.22 g of macroRAFT **3** was introduced in a Schlenk equipped with a magnetic stirring bar. In a second Schlenk flask were added a dispersion of rhodium complex **2a** (75 mg, 0.169 mmol) or **2b** (75 mg, 0.137 mmol) and styrene (1.73 g, 16.6 mmol for **2a**; 1.72g, 16.5 mmol for **2b**, argon-purged at 0 °C) in degassed water (3 mL), and an argon-purged solution of ACPA/NaHCO₃ (3.1 mg/3.1 mg) in water (2 mL). The reaction mixture was then purged again with argon for 15 min at 0 °C and added to the macroRAFT **3**, which had been placed in a thermostated oil bath at 80 °C. After 3 h of stirring under argon, an aliquot of the colloidal dispersion was withdrawn for ¹H NMR analysis (DMSO-*d*₆). A 99% conversion was determined and the polymerization was quenched by immersion of the flask in iced water.

Step 3: Core cross-linking with DEGDMA: synthesis of 5a and 5b.

To the Schlenk flask containing the R₀-(MAA₁₅-*co*-PEOMA₁₅)-*b*-(St₂₉₇-*co*-**2a-b**)-SC(S)SPr block copolymer **4a** or **4b** from step 2, degassed styrene (544 mg, 5.22 mmol), DEGDMA (108 mg, 0.447 mmol), deionized water (2 mL) and a degassed solution of ACPA (3.1 mg, 0.011 mmol) and NaHCO₃ (3.1 mg) in deionized water (1 mL) were added. The reaction mixture was purged for 15 min with argon at 0 °C and stirred at room temperature for 45 min, then placed in an oil bath thermostated at 80 °C. After 1 h 30 min stirring at 80 °C, a 98% conversion of the comonomers was determined by ¹H NMR (DMSO-*d*₆) and the polymerization was quenched by immersion of the flask in iced water. **5a**: 22.9% solid content, [Rh]: 0.0115 mol.L⁻¹. **5b**: 22.8% solid content, [Rh]: 0.0094 mol.L⁻¹

General procedure for hydrogenation with Rh-NHC molecular complex 7b

Styrene (1.04 g, 10 mmol), rhodium complex **7b** (5.8 mg, 0.01 mmol; substrate/Rh:1000/1) and decane (426 mg, 3 mmol) as internal standard were dissolved in toluene (1 mL) and placed in a 5 mL vial containing a magnetic stirring bar. The vial was placed in a steel reactor, which was purged 3 times with 10 bar of H₂, then charged with 20 bar of H₂. *Caution: high pressure hydrogenations should only be performed by suitably trained personnel.* The reaction mixture was then stirred at 80 °C for 6 h at a speed of 1200 rpm. After 1 h of resting at room temperature, the reactor was vented. The reaction mixture was filtered on silica, which was then rinsed with twice its volume of dichloromethane. It was then analysed by gas chromatography.

General procedure for biphasic hydrogenation with Rh-NHC^{mes}@CCM **5b**

A stock organic solution was prepared by mixing styrene (3.17 g, 30 mmol) and decane (1.26 g, 9 mmol) as internal standard in

40 mL of toluene, for a final substrate concentration of $7.5 \cdot 10^{-4}$ mol.mL⁻¹.

In a vial containing a magnetic stirring bar was added 0.5 mL of water containing Rh-NHC^{mes}@CCM **5b** (8.5 mg, $7.9 \cdot 10^{-8}$ mol of Rh), and 1 mL of the organic stock solution (substrate/Rh: 10 000/1). The vial was placed in a steel reactor, which was purged 3 times with 10 bar of H₂, then charged with 20 bar of H₂. The reaction mixture was then stirred at 80 °C for 6 h at a speed of 1200 rpm. The reactor was vented after 1 h of rest at room temperature. After overnight decantation, the organic layer was withdrawn by syringe and the aqueous phase was extracted twice with 0.5 mL of diethyl ether. The combined organic solutions were filtered through silica, and then analysed by gas chromatography. In order to perform the leaching measurements, the combined organic phases of one of the batches were not filtered through silica after decantation and phase separation.

Recycling experiments

To the aqueous phase containing the the Rh-NHC^{mes}@CCM **5b** was added a fresh portion (1 mL) of the organic stock solution. The vial was placed in a steel reactor and the hydrogenation reaction was set up as previously described. After reaction and overnight decantation, the aqueous phase was extracted twice with 0.5 mL of toluene instead of diethyl ether. One batch was filtered through silica for GC analysis, and the other one was left unfiltered for leaching measurements.

Author Contributions

S. S. Sambou, R. Hromov: synthesis and general labwork, validation; I. Ruzhylo: synthesis and general labwork, validation, writing (review); H. Wang: synthesis and general labwork, validation, funding acquisition, writing (review); A. Allandrieu, C. Sabatier: synthesis and general labwork; Y. Coppel: NMR investigation, reviewed the NMR draft section; J.-C. Daran: X-ray crystallography investigation, wrote the original X-ray crystallography draft section; F. Gayet: supervision, validation, writing (review); A. Labande: conceptualization, investigation, supervision, validation, writing (original draft); E. Manoury: conceptualization, funding acquisition, validation, writing (review); R. Poli: conceptualization, funding acquisition, writing (review).

Conflicts of interest

There are no conflicts to declare.

Acknowledgements

The authors are grateful to the Centre National de la Recherche Scientifique (CNRS) and the Institut Universitaire de France (IUF) for financial support. The authors also thank the China Scholarship Council for a Ph.D. fellowship to H.Wang. Mass spectrometry: the technical assistance provided by N. Martins-Froment of the ICT-FR 2599 (Toulouse, France - ict.ups-tlse.fr) is gratefully acknowledged.

Notes and references

‡ **5b*** was used in this recycling experiment. See Supplementary Information for pictures of **5b*** at a 1000/1 molar ratio after 1 run and after 5 runs.

- 1 M. Benaglia, *Recoverable and Recyclable Catalysts*, John Wiley & Sons, Ltd., Chichester, UK, 2009.
- 2 R. A. Sheldon, *Chem. Soc. Rev.*, 2012, **41**, 1437-1451.
- 3 B. Cornils, W. A. Herrmann, I. T. Horváth, W. Leitner, S. Mecking, H. Olivier-Bourbigou and D. Vogt, *Multiphase Homogeneous Catalysis*, Wiley-VCH Verlag GmbH & Co. KGaA, Weinheim, 2005.
- 4 I. T. Horváth and J. Rábai, *Science*, 1994, **266**, 72-75.
- 5 D. F. Foster, D. Gudmunsen, D. J. Adams, A. M. Stuart, E. G. Hope, D. J. Cole-Hamilton, G. P. Schwarz and P. Pogorzelec, *Tetrahedron*, 2002, **58**, 3901-3910.
- 6 T. Welton, *Chem. Rev.*, 1999, **99**, 2071-2084.
- 7 P. Wasserscheid and W. Keim, *Angew. Chem. Int. Ed.*, 2000, **39**, 3772-3789.
- 8 B. Cornils and W. A. Herrmann, *Aqueous-Phase Organometallics Catalysis*, WILEY-VCH Verlag GmbH&Co. KGaA, Weinheim, 2004.
- 9 P. H. Dixneuf and V. Cadierno, *Metal-Catalyzed Reactions in Water*, Wiley-VCH Verlag & Co. KGaA, Weinheim, 2013.
- 10 S. Liu and J. Xiao, in *Bridging Heterogeneous and Homogeneous Catalysis*, eds. L. Can and L. Yan, Wiley-VCH Verlag GmbH & Co. KGaA, Weinheim, 2014, DOI: 10.1002/9783527675906.ch6, pp. 201-252.
- 11 T. Kitanosono, K. Masuda, P. Xu and S. Kobayashi, *Chem. Rev.*, 2018, **118**, 679-746.
- 12 B. Cornils, *Org. Process Res. Dev.*, 1998, **2**, 121-127.
- 13 F. Joó, *Acc. Chem. Res.*, 2002, **35**, 738-745.
- 14 L. Gao, K. Kojima and H. Nagashima, *Tetrahedron*, 2015, **71**, 6414-6423.
- 15 N. T. Thanh Chau, S. Menuel, S. Colombel-Rouen, M. Guerrero, E. Monflier, K. Philippot, A. Denicourt-Nowicki and A. Roucoux, *RSC Adv.*, 2016, **6**, 108125-108131.
- 16 C. Wai-Chung, L. Chak-Po, L. Cheng and L. Yin-Shan, *J. Organomet. Chem.*, 1994, **464**, 103-106.
- 17 K. Cousin, T. Vanbésien, E. Monflier and F. Hapiot, *Catal. Commun.*, 2019, **125**, 37-42.
- 18 S. Bhama, T. R. Sibakoti, J. B. Jasinski and F. P. Zamborini, *ChemCatChem*, 2020, **12**, 2253-2261.
- 19 A. Behr, M. Urschey and V. A. Brehme, *Green Chem.*, 2003, **5**, 198-204.
- 20 F. Hapiot and E. Monflier, *Catalysts*, 2017, **7**, 173.
- 21 G. La Sorella, G. Strukul and A. Scarso, *Green Chem.*, 2015, **17**, 644-683.
- 22 B. H. Lipshutz, S. Ghorai and M. Cortes-Clerget, *Chem.–Eur. J.*, 2018, **24**, 6672-6695.
- 23 M. Cortes-Clerget, N. Akporji, J. Zhou, F. Gao, P. Guo, M. Parmentier, F. Gallou, J.-Y. Berthon and B. H. Lipshutz, *Nature Communications*, 2019, **10**, 2169.
- 24 T.-L. Nghiem, D. Coban, S. Tjaberings and A. H. Gröschel, *Polymers*, 2020, **12**, 2190.
- 25 T. Terashima, M. Kamigaito, K.-Y. Baek, T. Ando and M. Sawamoto, *J. Am. Chem. Soc.*, 2003, **125**, 5288-5289.
- 26 A. D. Ilevins, X. Wang, A. O. Moughton, J. Skey and R. K. O'Reilly, *Macromolecules*, 2008, **41**, 2998-3006.
- 27 P. Cotanda, A. Lu, J. P. Patterson, N. Petzetakis and R. K. O'Reilly, *Macromolecules*, 2012, **45**, 2377-2384.
- 28 Y. Liu, Y. Wang, Y. Wang, J. Lu, V. Piñón and M. Weck, *J. Am. Chem. Soc.*, 2011, **133**, 14260-14263.
- 29 M. Zheng, Z. Sun, Z. Xie and X. Jing, *Chem.–Asian J.*, 2013, **8**, 2807-2812.
- 30 X. Zhang, A. F. Cardozo, S. Chen, W. Zhang, C. Julcour, M. Lansalot, J. F. Blanco, F. Gayet, H. Delmas, B. Charleux, E.

- Manoury, F. D'Agosto and R. Poli, *Chem.– Eur. J.*, 2014, **20**, 15505-15517.
- 31 A. F. Cardozo, C. Julcour, L. Barthe, J.-F. Blanco, S. Chen, F. Gayet, E. Manoury, X. Zhang, M. Lansalot, B. Charleux, F. D'Agosto, R. Poli and H. Delmas, *J. Catal.*, 2015, **324**, 1-8.
 - 32 S. Chen, E. Manoury, F. Gayet and R. Poli, *Polymers (Basel)*, 2016, **8**, 26.
 - 33 A. Joumaa, S. Chen, S. Vincendeau, F. Gayet, R. Poli and E. Manoury, *Mol. Catal.*, 2017, **438**, 267-271.
 - 34 E. Lobry, A. F. Cardozo, L. Barthe, J.-F. Blanco, H. Delmas, S. Chen, F. Gayet, X. Zhang, M. Lansalot, F. D'Agosto, R. Poli, E. Manoury and C. Julcour, *J. Catal.*, 2016, **342**, 164-172.
 - 35 S. Chen, F. Gayet, E. Manoury, A. Joumaa, M. Lansalot, F. D'Agosto and R. Poli, *Chem.– Eur. J.*, 2016, **22**, 6302-6313.
 - 36 A. Joumaa, F. Gayet, E. J. Garcia-Suarez, J. Himmelstrup, A. Riisager, R. Poli and E. Manoury, *Polymers*, 2020, **12**, 1107.
 - 37 H. Wang, L. Vendrame, C. Fliedel, S. Chen, F. Gayet, E. Manoury, X. Zhang, F. D'Agosto, M. Lansalot and R. Poli, *Macromolecules*, 2020, **53**, 2198-2208.
 - 38 S. Díez-González, *N-Heterocyclic Carbenes: From Laboratory Curiosities to Efficient Synthetic Tools*, the Royal Society of Chemistry, Cambridge, 2 edn., 2017.
 - 39 D. Bourissou, O. Guerret, F. P. Gabbaï and G. Bertrand, *Chem. Rev.*, 2000, **100**, 39-92.
 - 40 P. de Frémont, N. Marion and S. P. Nolan, *Coord. Chem. Rev.*, 2009, **253**, 862-892.
 - 41 S. Díez-González and S. P. Nolan, *Coord. Chem. Rev.*, 2007, **251**, 874-883.
 - 42 F. E. Hahn and M. C. Jahnke, *Angew. Chem. Int. Ed.*, 2008, **47**, 3122-3172.
 - 43 H. V. Huynh, *Chem. Rev.*, 2018, **118**, 9457-9492.
 - 44 L. Benhamou, E. Chardon, G. Lavigne, S. Bellemin-Lapponaz and V. César, *Chem. Rev.*, 2011, **111**, 2705-2733.
 - 45 F. Glorius, *N-Heterocyclic Carbenes in Transition Metal Catalysis*, Springer Verlag, Berlin Heidelberg, 2007.
 - 46 S. Díez-González, N. Marion and S. P. Nolan, *Chem. Rev.*, 2009, **109**, 3612-3676.
 - 47 W. A. Herrmann, *Angew. Chem. Int. Ed.*, 2002, **41**, 1290-1309.
 - 48 M. T. Zarka, M. Bortenschlager, K. Wurst, O. Nuyken and R. Weberskirch, *Organometallics*, 2004, **23**, 4817-4820.
 - 49 R. Lambert, A.-L. Wirocius, S. Garmendia, P. Berto, J. Vignolle and D. Taton, *Polym. Chem.*, 2018, **9**, 3199-3204.
 - 50 R. Lambert, A.-L. Wirocius, J. Vignolle and D. Taton, *Polym. Chem.*, 2019, **10**, 460-466.
 - 51 M. Biewend, S. Neumann, P. Michael and W. H. Binder, *Polym. Chem.*, 2019, **10**, 1078-1088.
 - 52 C. Boztepe, A. Künkül and N. Gürbüz, *J. Mol. Struct.*, 2020, **1209**, 127948.
 - 53 A. Donner, B. Trepka, S. Theiss, F. Immler, J. Traber and S. Polarz, *Langmuir*, 2019, **35**, 16514-16520.
 - 54 Y. Lei, M. Fan, G. Lan and G. Li, *Appl. Organomet. Chem.*, 2020, **34**, e5794.
 - 55 Y. Lei, G. Lan, M. Fan and G. Li, *Catal. Commun.*, 2020, **140**, 106007.
 - 56 N. Pentela, V. Gayathri and D. Samanta, *J. Organomet. Chem.*, 2020, **913**, 121196.
 - 57 P. Puthiaraj, S. Ravi, K. Yu and W.-S. Ahn, *Appl. Catal., B*, 2019, **251**, 195-205.
 - 58 Y. Shen, Q. Zheng, H. Zhu and T. Tu, *Adv. Mater.*, 2020, **32**, 1905950.
 - 59 R. Wang, L. Qin, X. Wang, B. Chen, Y. Zhao and G. Gao, *Catal. Commun.*, 2020, **138**, 105924.
 - 60 X. Wang, Q. Dong, Z. Xu, Y. Wu, D. Gao, Y. Xu, C. Ye, Y. Wen, A. Liu, Z. Long and G. Chen, *Chem. Eng. J.*, 2021, **403**, 126460.
 - 61 N. Debono, A. Labande, E. Manoury, J.-C. Daran and R. Poli, *Organometallics*, 2010, **29**, 1879-1882.
 - 62 S. Gülcemal, A. Labande, J.-C. Daran, B. Cetinkaya and R. Poli, *Eur. J. Inorg. Chem.*, 2009, **2009**, 1806-1815.
 - 63 A. Labande, N. Debono, A. Sournia-Saquet, J.-C. Daran and R. Poli, *Dalton Trans.*, 2013, **42**, 6531-6537.
 - 64 P. Loxq, J.-C. Daran, E. Manoury, R. Poli and A. Labande, *Eur. J. Inorg. Chem.*, 2015, **2015**, 609-616.
 - 65 J. Wolf, A. Labande, J.-C. Daran and R. Poli, *J. Organomet. Chem.*, 2006, **691**, 433-443.
 - 66 J. Wolf, A. Labande, J.-C. Daran and R. Poli, *Eur. J. Inorg. Chem.*, 2007, **2007**, 5069-5079.
 - 67 S. Gülcemal and B. Çetinkaya, in *N-Heterocyclic Carbenes: From Laboratory Curiosities to Efficient Synthetic Tools*, ed. S. Díez-González, The Royal Society of Chemistry, Cambridge, 2nd edn., 2017, DOI: 10.1039/9781782626817-00484, ch. 13, pp. 484-533.
 - 68 J. M. Praetorius and C. M. Crudden, *Dalton Trans.*, 2008, **2008**, 4079-4094.
 - 69 D. Zhao, L. Candish, D. Paul and F. Glorius, *ACS Catal.*, 2016, **6**, 5978-5988.
 - 70 D. P. Allen, C. M. Crudden, L. A. Calhoun and R. Wang, *J. Organomet. Chem.*, 2004, **689**, 3203-3209.
 - 71 D. P. Allen, C. M. Crudden, L. A. Calhoun, R. Wang and A. Decken, *J. Organomet. Chem.*, 2005, **690**, 5736-5746.
 - 72 W. A. Herrmann, G. D. Frey, E. Herdtweck and M. Steinbeck, *Adv. Synth. Catal.*, 2007, **349**, 1677-1691.
 - 73 D. Baskakov, W. A. Herrmann, E. Herdtweck and S. D. Hoffmann, *Organometallics*, 2007, **26**, 626-632.
 - 74 P. Li, W. A. Herrmann and F. E. Kühn, *ChemCatChem*, 2013, **5**, 3324-3329.
 - 75 P. D. Newman, K. J. Cavell, A. J. Hallett and B. M. Kariuki, *Dalton Trans.*, 2011, **40**, 8807-8813.
 - 76 J. J. Dunsford, D. S. Tromp, K. J. Cavell, C. J. Elsevier and B. M. Kariuki, *Dalton Trans.*, 2013, **42**, 7318-7329.
 - 77 S. Doherty, J. G. Knight, M. A. Carroll, A. R. Clemmet, J. R. Ellison, T. Backhouse, N. Holmes, L. A. Thompson and R. A. Bourne, *RSC Adv.*, 2016, **6**, 73118-73131.
 - 78 J. Pyun, E. Drockenmüller, T. P. Russell, J. L. Hedrick, C. J. Hawker and J. M. J. Frechet, *PMSE Prepr.*, 2004, **91**, 868.
 - 79 I. Benaissa, R. Taakili, N. Lukan and Y. Canac, *Dalton Trans.*, 2017, **46**, 12293-12305.
 - 80 A. Bittermann, P. Härter, E. Herdtweck, S. D. Hoffmann and W. A. Herrmann, *J. Organomet. Chem.*, 2008, **693**, 2079-2090.
 - 81 C. Mejuto, G. Guisado-Barrios and E. Peris, *Organometallics*, 2014, **33**, 3205-3211.
 - 82 S. L. Canning, G. N. Smith and S. P. Armes, *Macromolecules*, 2016, **49**, 1985-2001.
 - 83 B. Charleux, G. Delaittre, J. Rieger and F. D'Agosto, *Macromolecules*, 2012, **45**, 6753-6765.
 - 84 F. D'Agosto, J. Rieger and M. Lansalot, *Angew. Chem. Int. Ed.*, 2020, **59**, 8368-8392.
 - 85 N. J. Warren and S. P. Armes, *J. Am. Chem. Soc.*, 2014, **136**, 10174-10185.
 - 86 S. Chen, A. F. Cardozo, C. Julcour, J.-F. Blanco, L. Barthe, F. Gayet, M. Lansalot, F. D'Agosto, H. Delmas, E. Manoury and R. Poli, *Polymer*, 2015, **72**, 327-335.
 - 87 A. S. Andreev and V. Livadaris, *J. Phys. Chem. C*, 2017, **121**, 14108-14119.
 - 88 B. L. Tran, J. L. Fulton, J. C. Linehan, J. A. Lercher and R. M. Bullock, *ACS Catal.*, 2018, **8**, 8441-8449.
 - 89 H. Wang, A. M. Fiore, C. Fliedel, E. Manoury, K. Philippot, M. M. Dell'Anna, P. Mastrolilli and R. Poli, *Nanoscale Adv.*, 2021, **3**, 2554-2566.
 - 90 Y. D. Lahneche, A. Lachgar, C. Mouton, J.-C. Daran, E. Manoury, R. Poli, M. Benslimane, A. Labande and E. Deydier, *Inorg. Chim. Acta*, 2019, **492**, 91-97.
 - 91 L. E. Marbella and J. E. Millstone, *Chem. Mater.*, 2015, **27**, 2721-2739.
 - 92 X.-Y. Yu, H. Sun, B. O. Patrick and B. R. James, *Eur. J. Inorg. Chem.*, 2009, **2009**, 1752-1758.
 - 93 T. Boursier, I. Chaduc, J. Rieger, F. D'Agosto, M. Lansalot and B. Charleux, *Polym. Chem.*, 2011, **2**, 355-362.
 - 94 G. Sheldrick, *Acta Crystallogr., Sect. A*, 2015, **71**, 3-8.
 - 95 G. Sheldrick, *Acta Crystallogr., Sect. C*, 2015, **71**, 3-8.
 - 96 L. Farrugia, *J. Appl. Crystallogr.*, 1997, **30**, 565.

Amphiphilic Polymeric Nanoreactors Containing Rh(I)-NHC Complexes for the Aqueous Biphasic Hydrogenation of Alkenes

Sasaline Salomon Sambou,^a Roman Hromov,^a Illia Ruzhylo,^a Hui Wang,^a Audrey Allandrieu,^a Cassandra Sabatier,^a Yannick Coppel,^a Jean-Claude Daran,^a Florence Gayet,^a Agnès Labande,^{*a} Eric Manoury^{*a} and Rinaldo Poli^{*a,b}

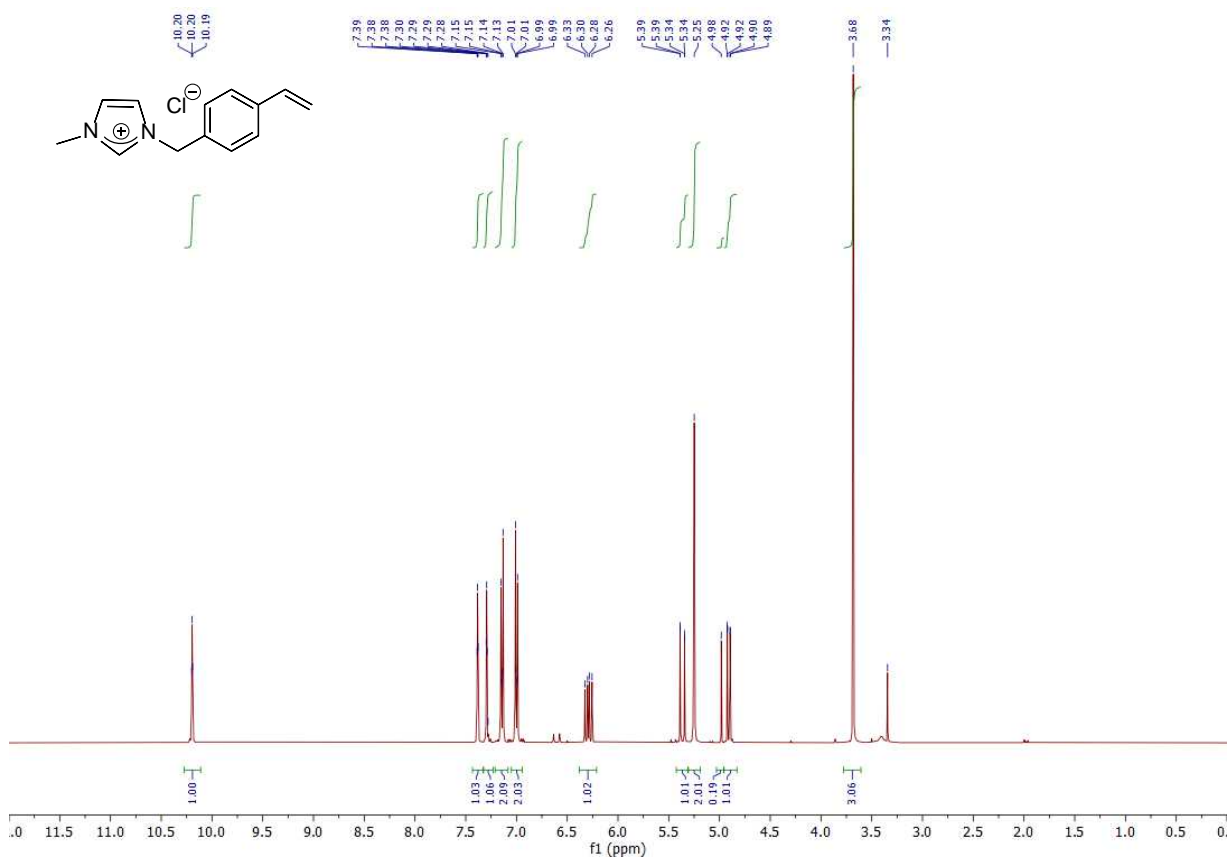
^a LCC-CNRS, Université de Toulouse, CNRS, INPT, 205 route de Narbonne, 31077 Toulouse, France. E-mail: agnes.labande@lcc-toulouse.fr; eric.manoury@lcc-toulouse.fr; rinaldo.poli@lcc-toulouse.fr; Fax: +33-5-61-55-30-03; Tel: ++33-5-61-33-31-00.

^b Institut Universitaire de France, 1, rue Descartes, 75231 Paris, France.

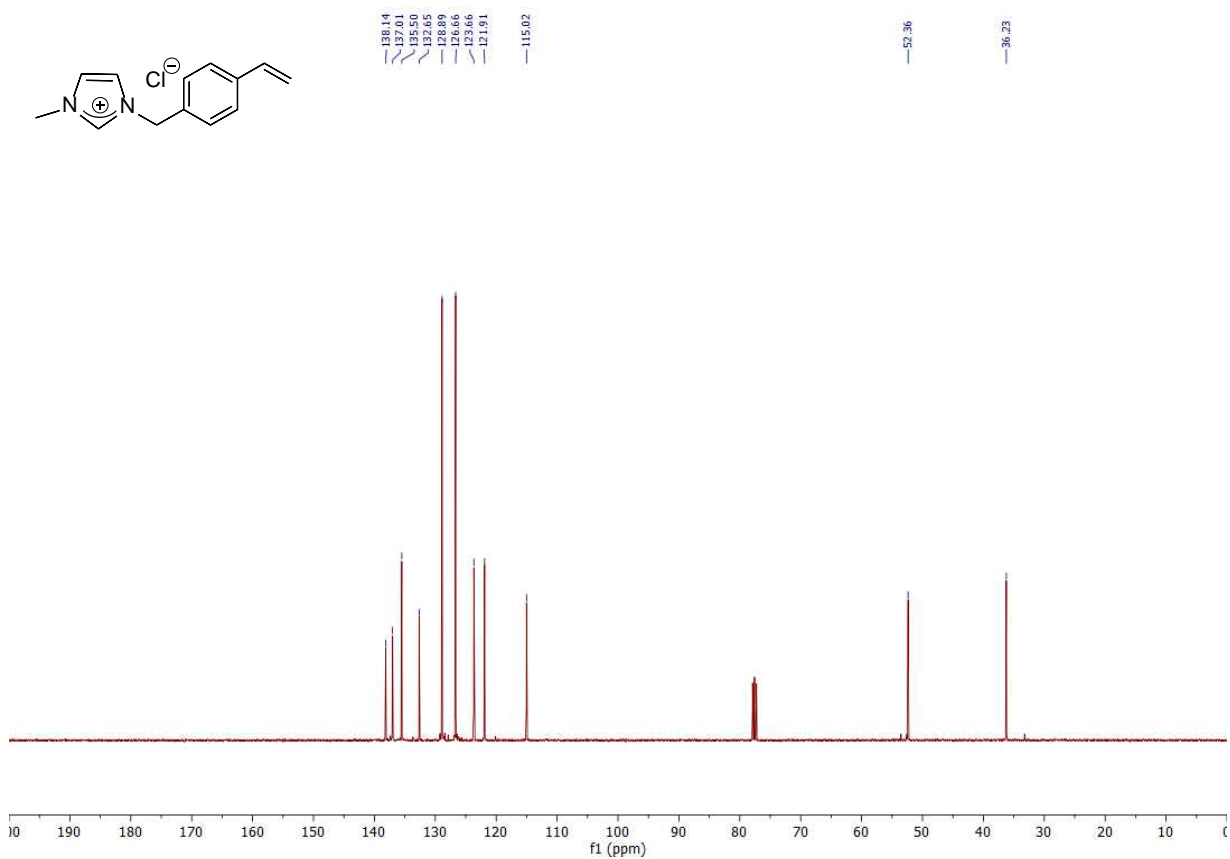
NMR analyses	Page S1
Unless otherwise stated, all spectra were recorded in CDCl ₃ on a Bruker Avance III 400 apparatus, operating at 400.16 MHz (¹ H) or 100.63 MHz (¹³ C).	
¹ H and ¹³ C NMR spectra of compound 1a	Page S1
¹ H and ¹³ C NMR spectra of compound 1b	Page S2
¹ H and ¹³ C NMR spectra of polymerizable rhodium(I) complex 2a	Page S3
¹ H and ¹³ C NMR spectra of polymerizable rhodium(I) complex 2b	Page S4
¹ H and ¹³ C NMR spectra of ¹³ C-labelled polymerizable rhodium(I) complex 2b*	Page S5
¹ H and ¹³ C NMR spectra of compound 6b	Page S6
¹ H and ¹³ C NMR spectra of model rhodium(I) complex 7b	Page S7
¹ H-MAS NMR spectrum (Avance III 400WB) of nanoreactors Rh-NHC ^{mes} @CCM 5b*	Page S8
¹ H-DFSE-MAS NMR spectrum of 5b* with ¹ H NMR spectrum of 2b* in THF- <i>d</i> ₈	Page S8
¹³ C-MAS NMR spectrum (Avance III 400WB) of nanoreactors Rh-NHC ^{mes} @CCM 5b*	Page S9
¹³ C-MAS NMR spectrum of 5b* with ¹³ C NMR spectrum of 2b* in THF- <i>d</i> ₈	Page S9
¹³ C-MAS NMR spectrum of nanoreactors Rh-NHC ^{mes} @CCM 5b* recovered after 5 runs hydrogenation	Page S10
DLS analyses Page S11	
DLS analyses of Rh-NHC ^{Me} @M 4a and Rh-NHC ^{mes} @M 4b , 45 μm filter	Page S11
DLS analyses of Rh-NHC ^{mes} @CCM 5a and Rh-NHC ^{mes} @CCM 5b , 45 μm filter	Page S11
DLS analyses of Rh-NHC ^{mes} @CCM 5b after hydrogenation, 45 μm filter	Page S11
TEM analyses Page S12	
TEM images of Rh-NHC ^{mes} @M 4b	Page S12
TEM images of Rh-NHC ^{mes} @CCM 5b	Page S12
Size distribution of Rh-NHC ^{mes} @CCM 5b	Page S13
TEM images of Rh-NHC ^{mes} @CCM 5b after 5 catalytic runs	Page S13
Photos of catalytic mixtures Page S14	
7b under “wet toluene”, “on-water” or toluene/DME conditions after hydrogenation	Page S14
7b with “blank” CCMs after 1 run of hydrogenation	Page S14
5b* after 1 and 5 runs of hydrogenation	Page S14
X-Ray diffraction analyses Page S15	
Table 1 – Crystal data and structure refinement	Page S15
Table 2 – Bond lengths [Å] and angles [°] for 2a	Page S16
Table 3 – Bond lengths [Å] and angles [°] for 2b	Page S17

NMR analyses

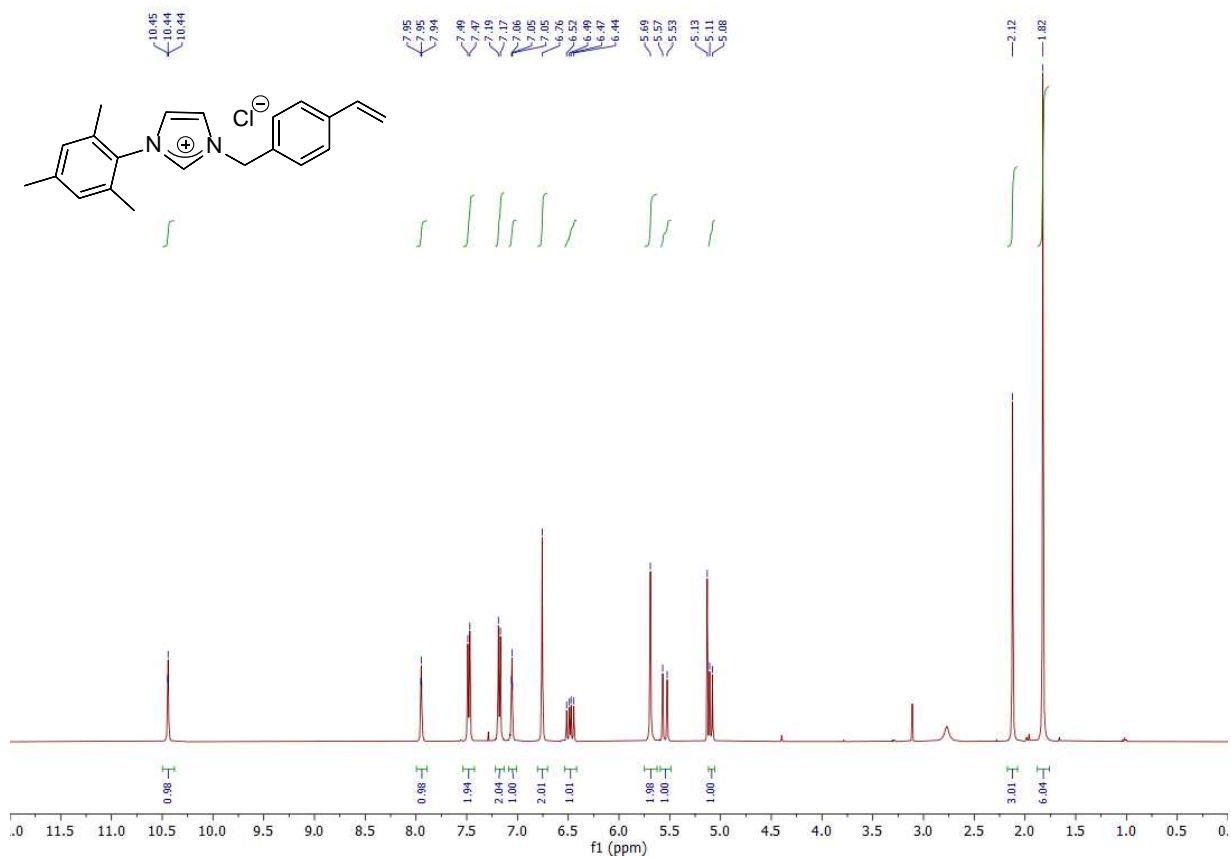
^1H NMR spectrum of compound **1a**



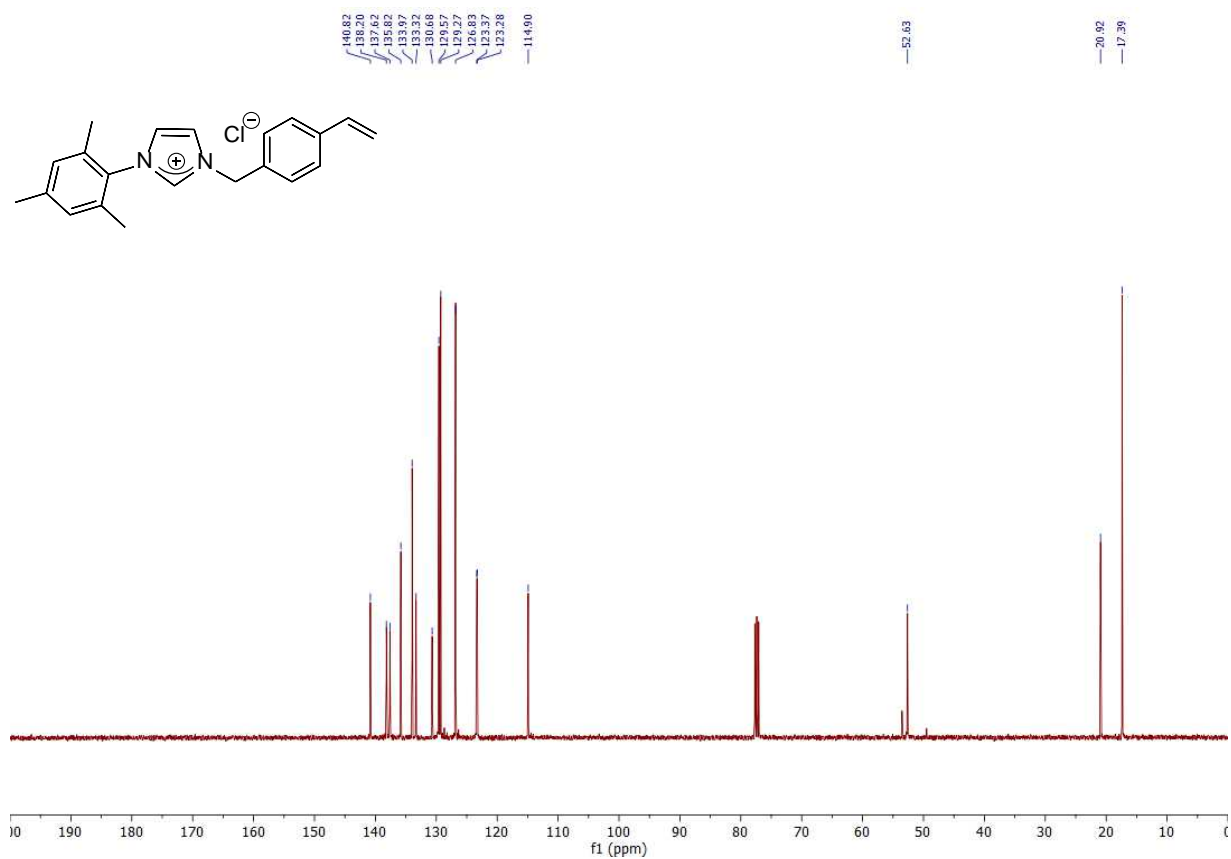
^{13}C NMR spectrum of compound **1a**



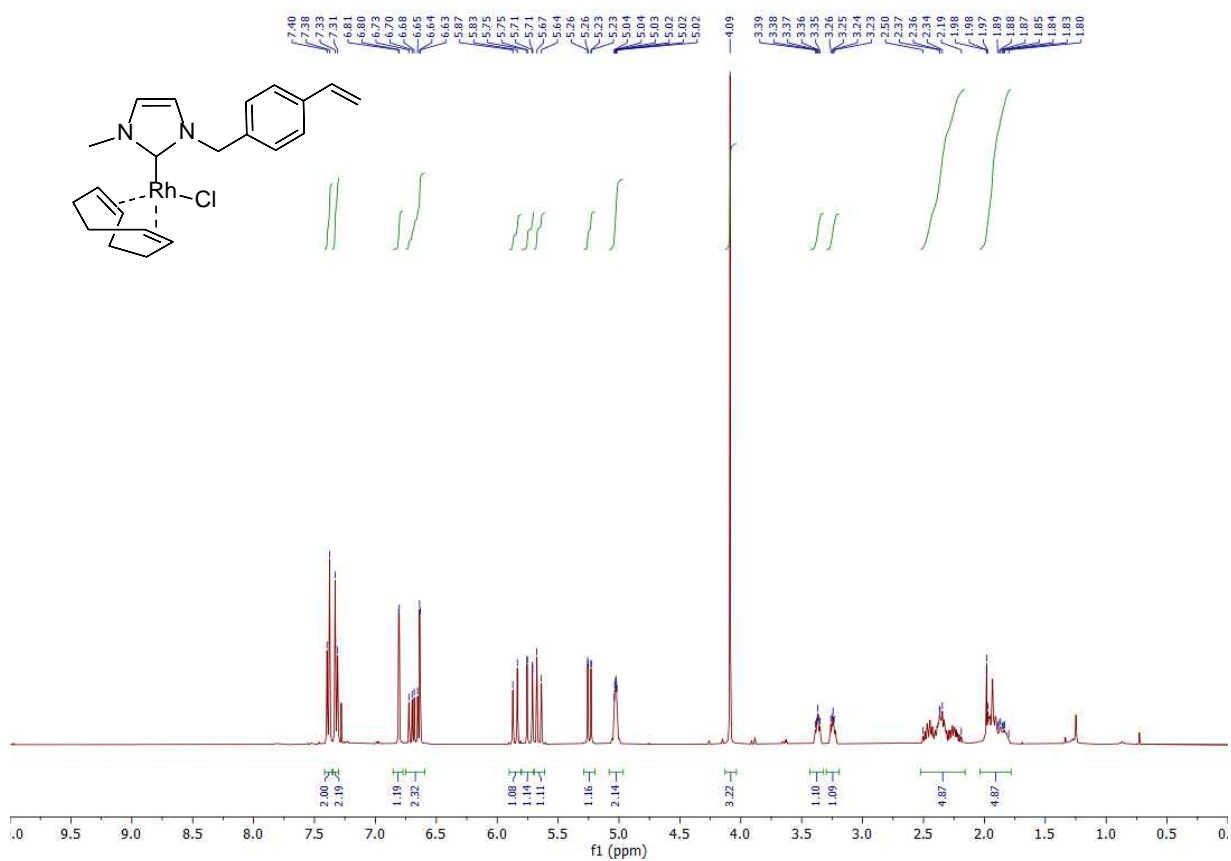
^1H NMR spectrum of compound **1b**



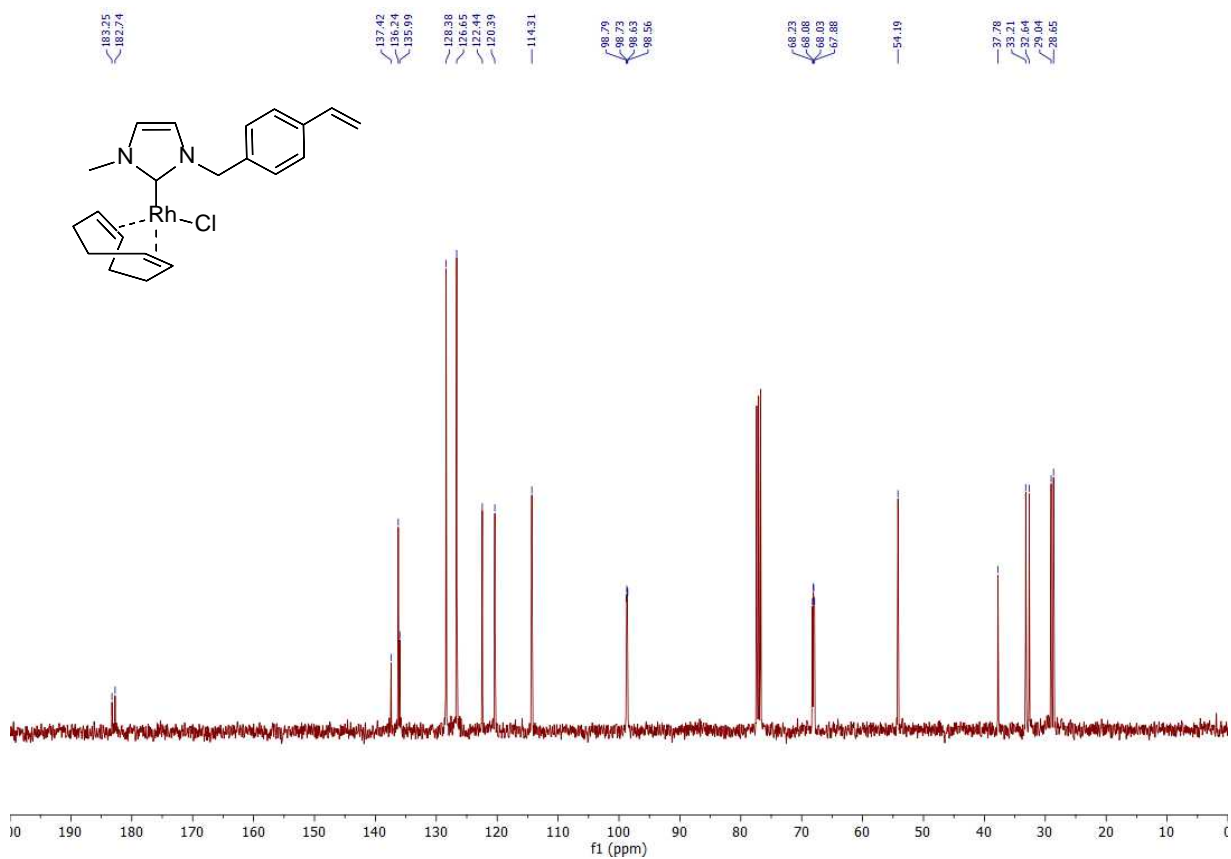
^{13}C NMR spectrum of compound **1b**



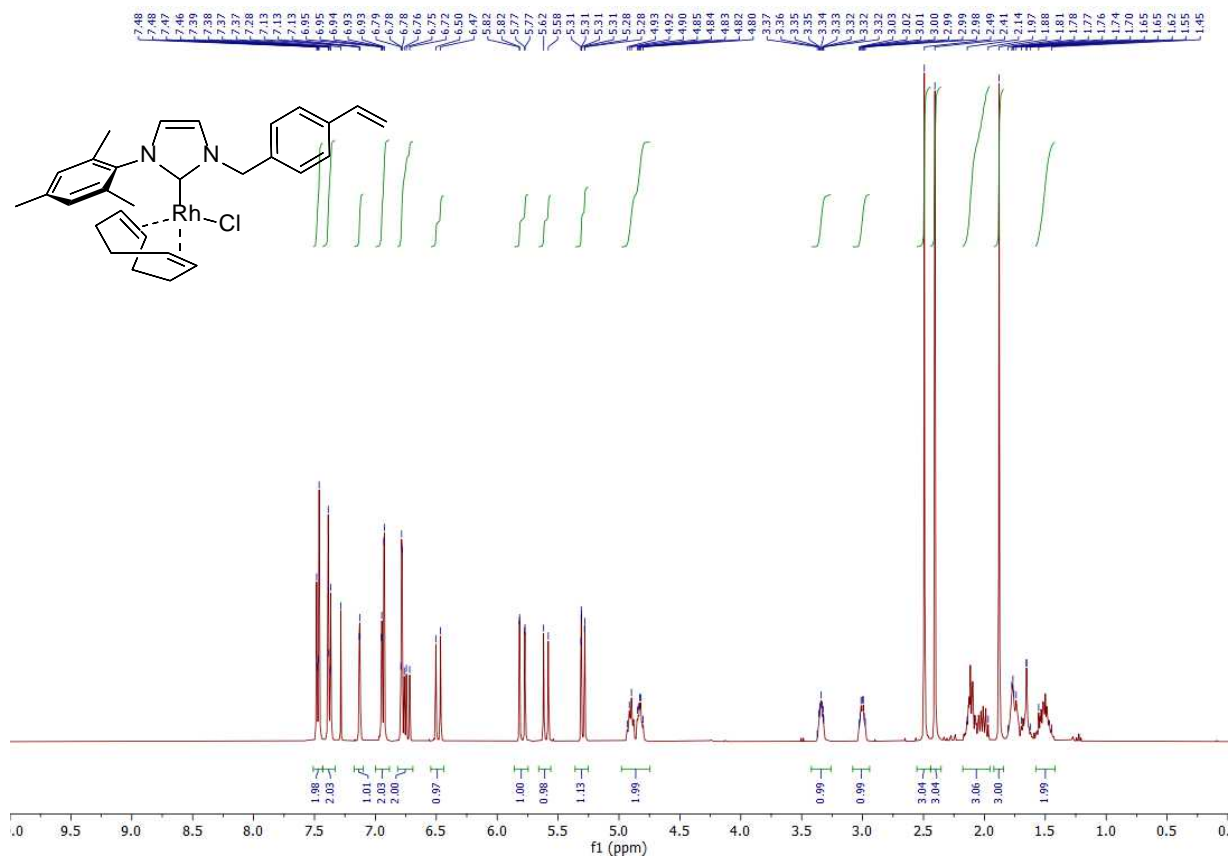
^1H NMR spectrum of polymerizable rhodium(I) complex **2a**



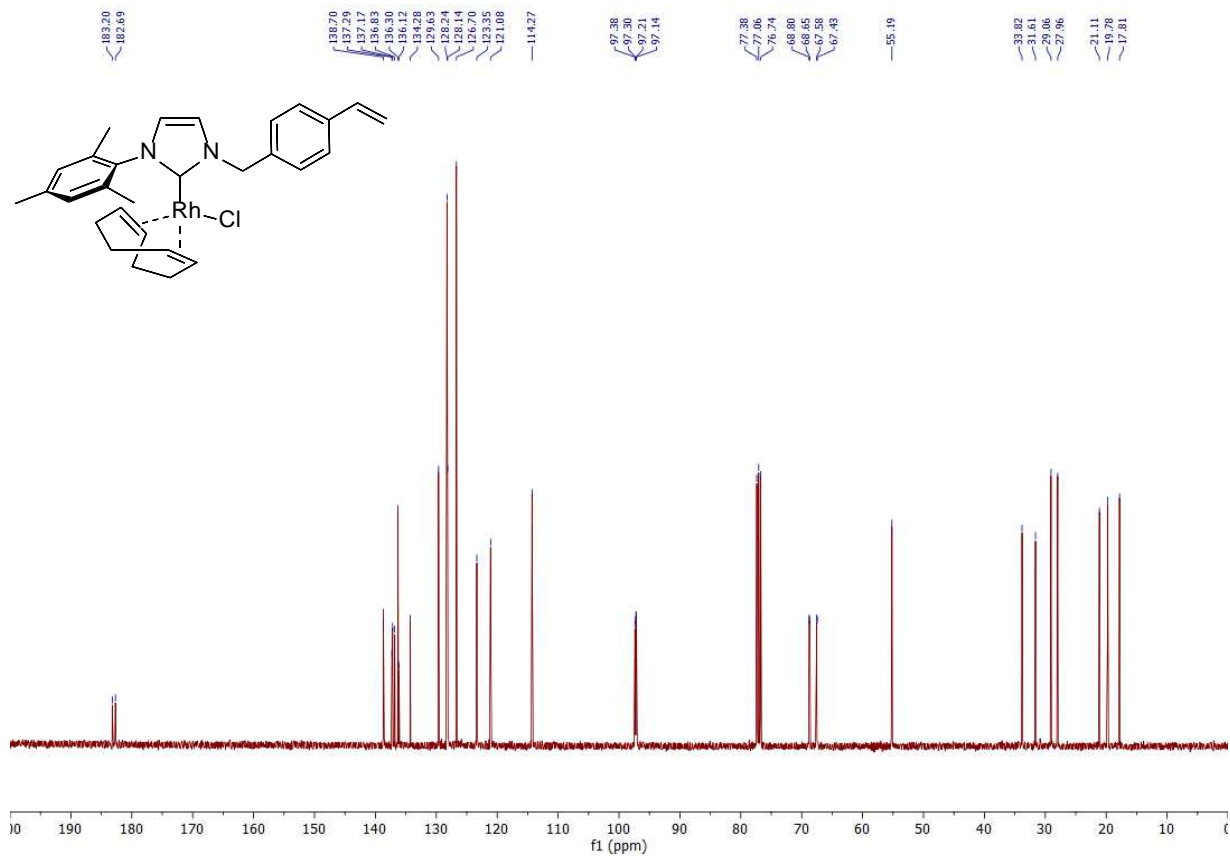
^{13}C NMR spectrum of polymerizable rhodium(I) complex **2a**



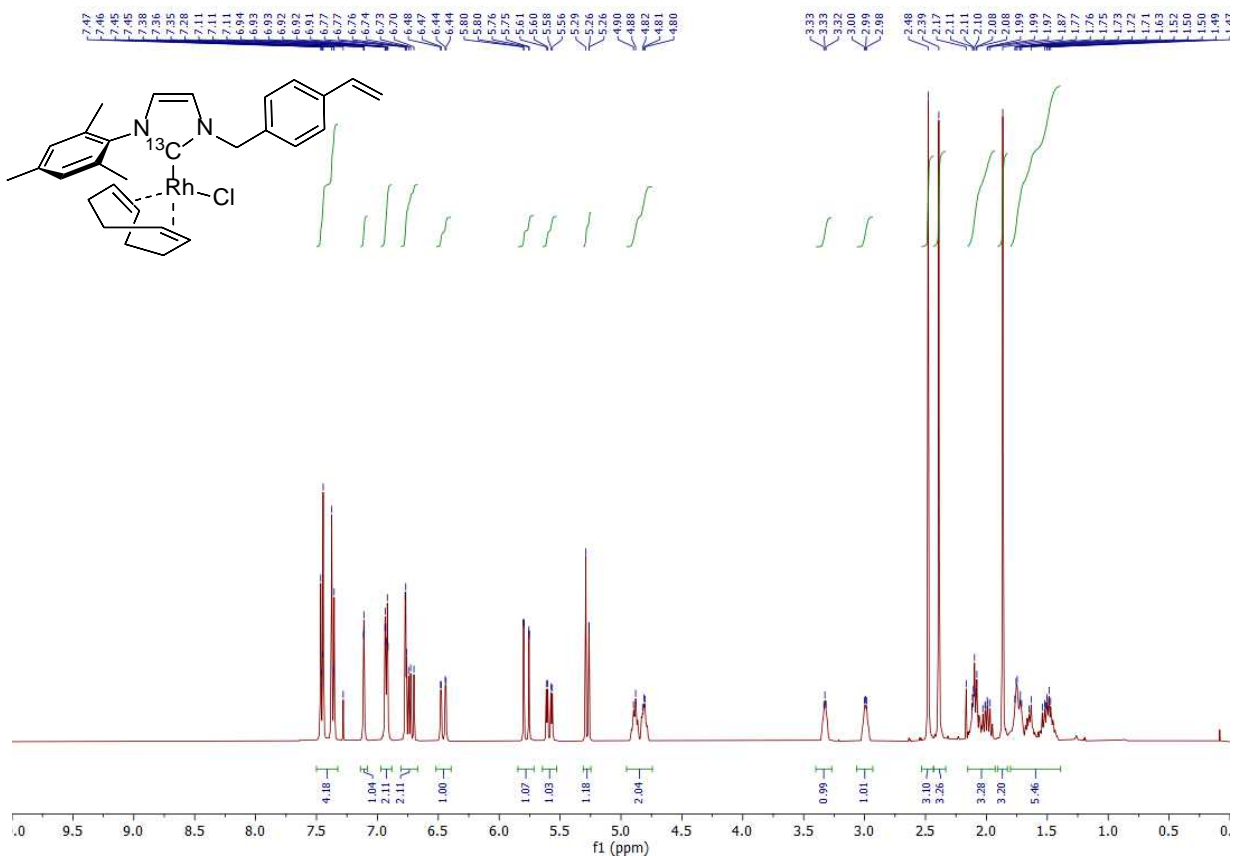
¹H NMR spectrum of polymerizable rhodium(I) complex **2b**



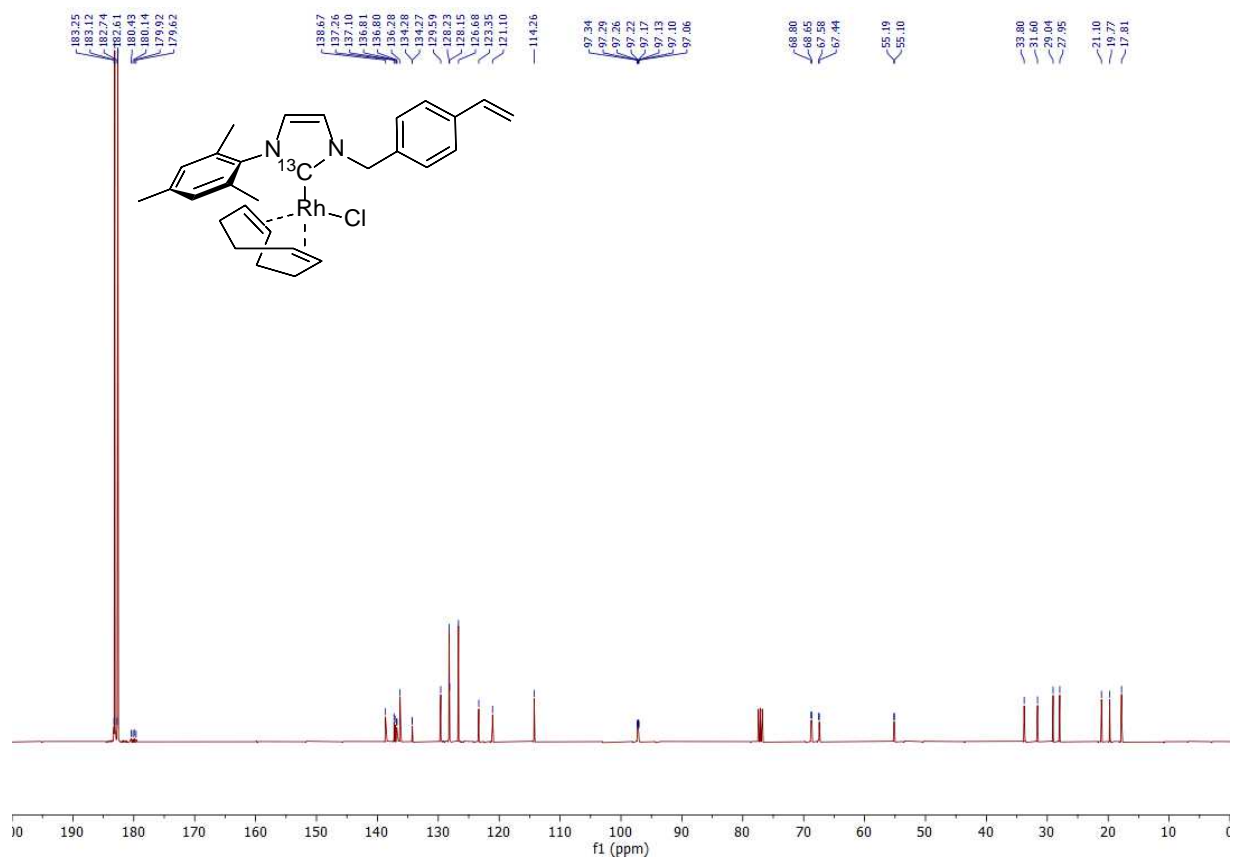
¹³C NMR spectrum of polymerizable rhodium(I) complex **2b**



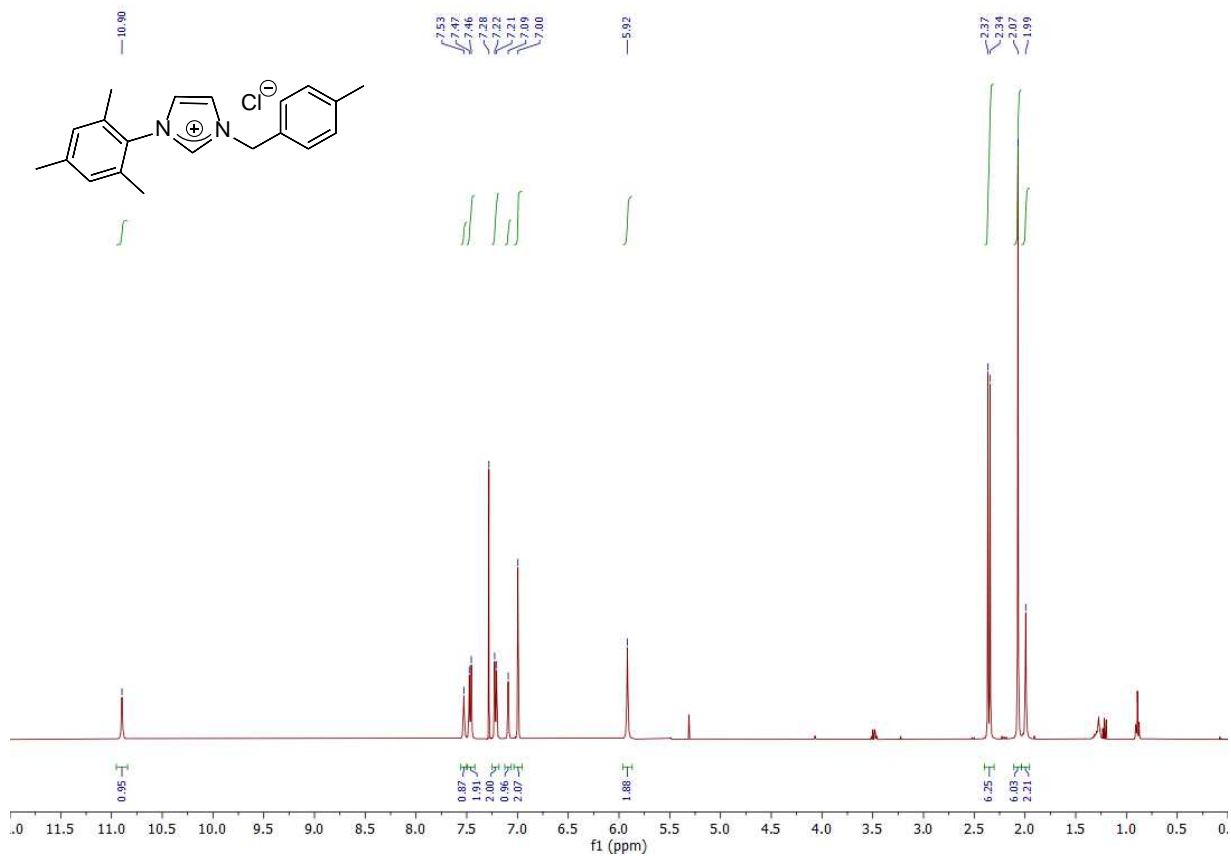
^1H NMR spectrum of ^{13}C -labelled polymerizable rhodium(I) complex **2b***



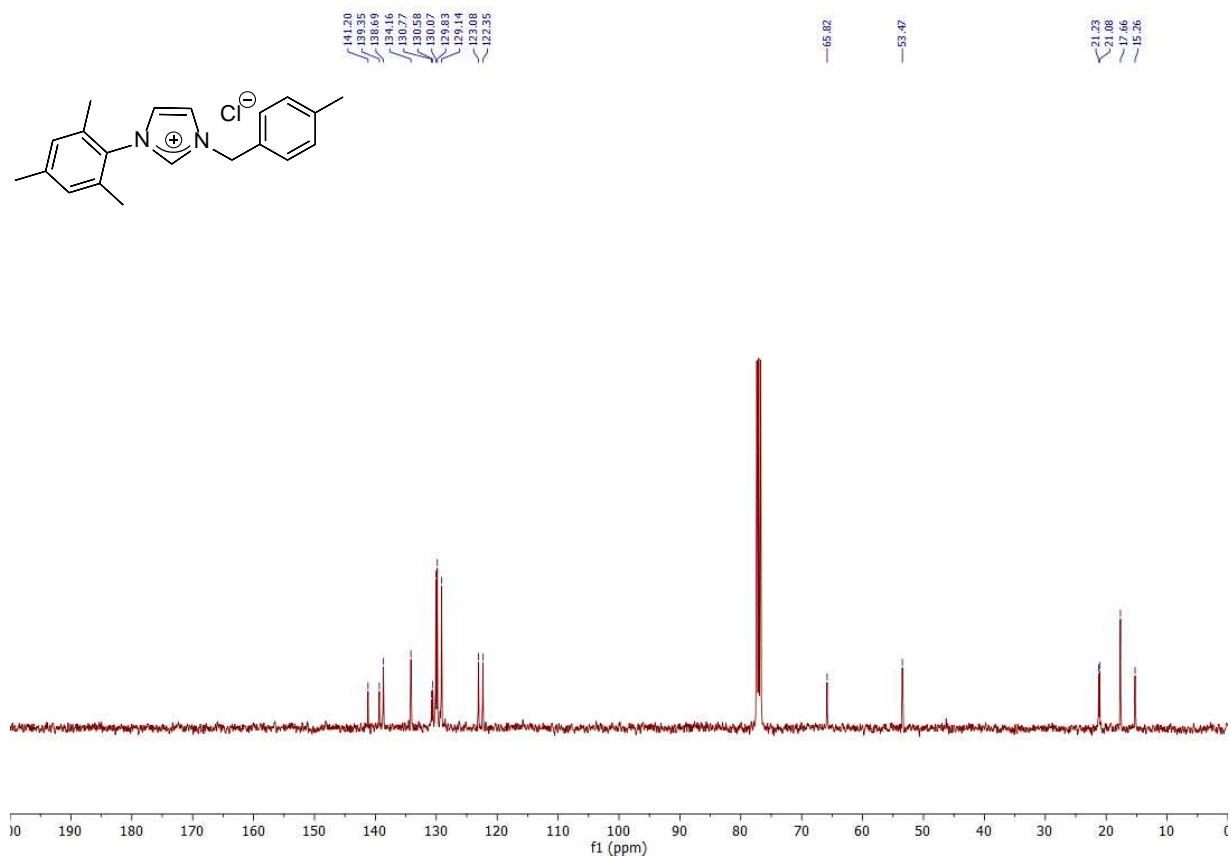
^{13}C NMR spectrum of ^{13}C -labelled polymerizable rhodium(I) complex **2b***



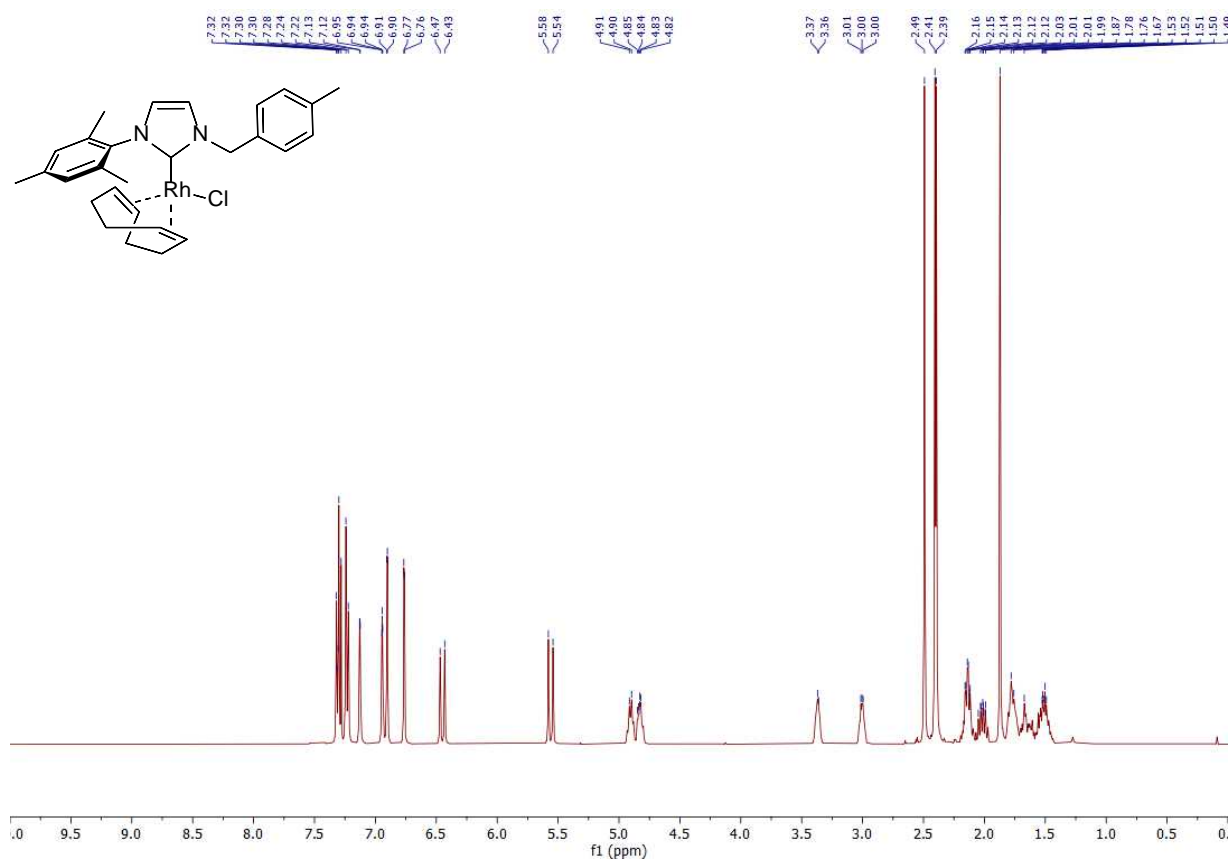
^1H NMR spectrum of compound **6b**



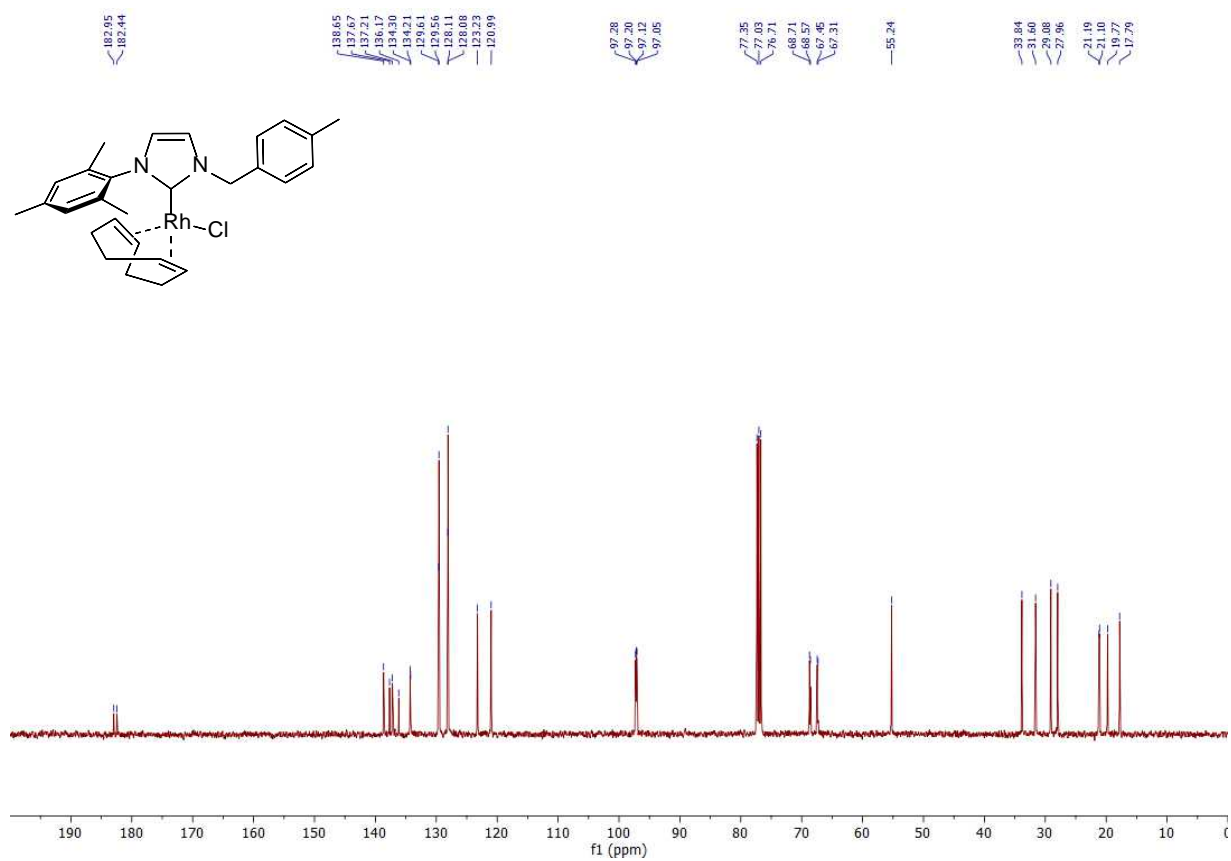
^{13}C NMR spectrum of compound **6b**



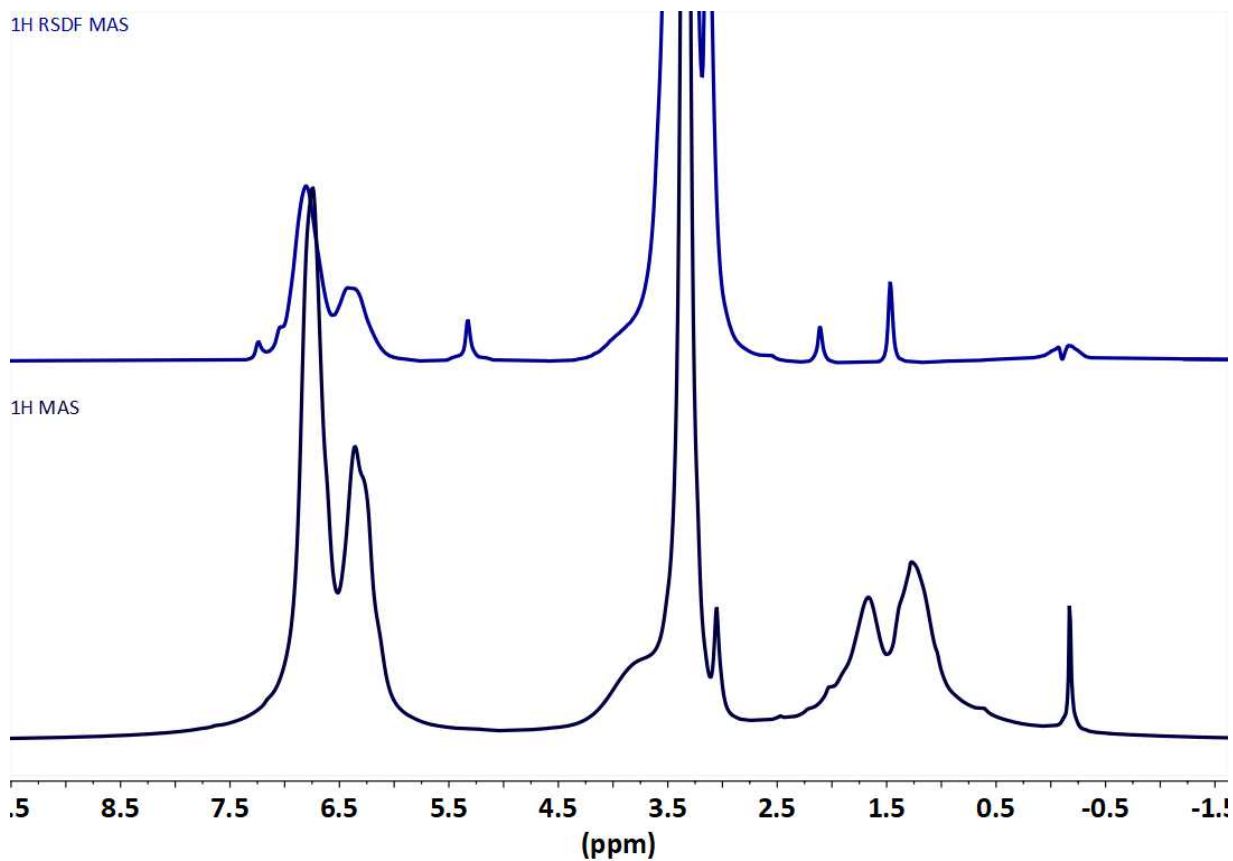
^1H NMR spectrum of model rhodium(I) complex **7b**



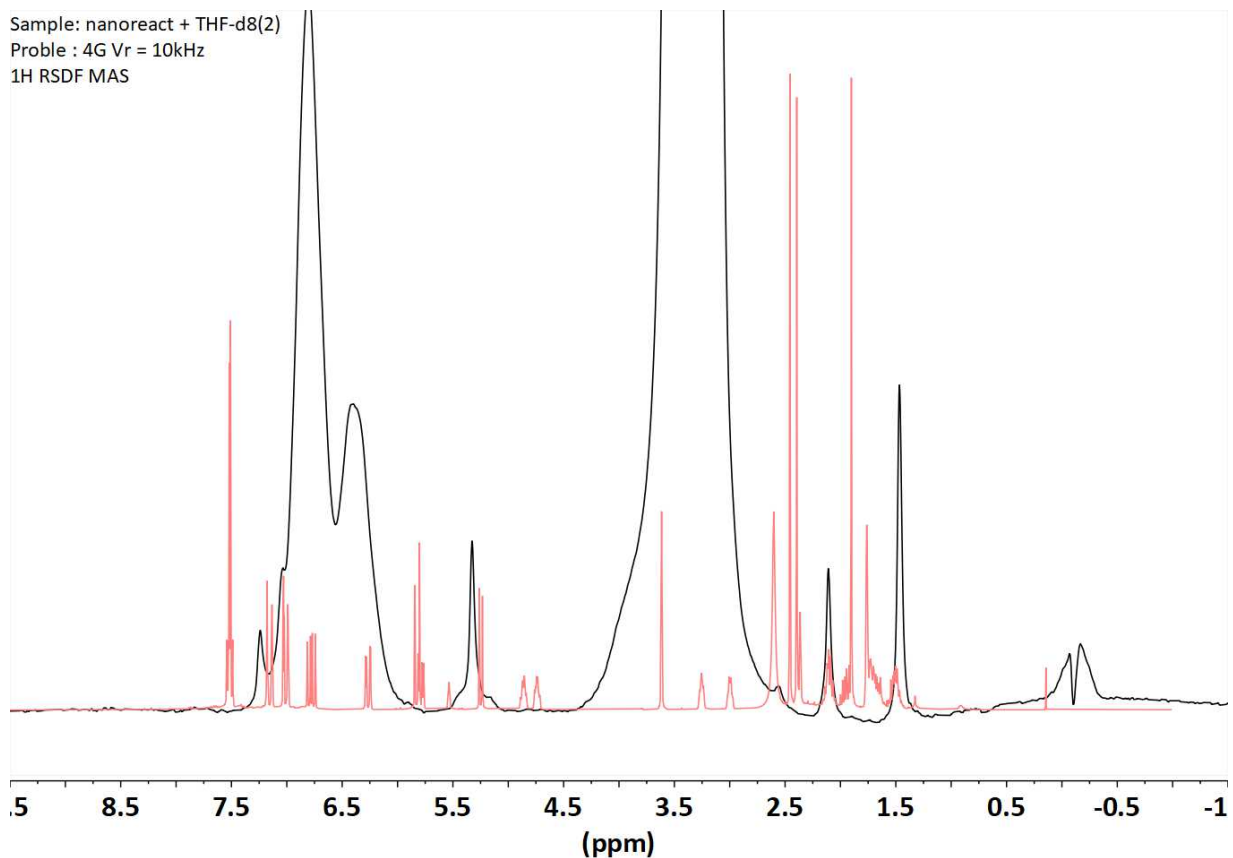
^{13}C NMR spectrum of model rhodium(I) complex **7b**



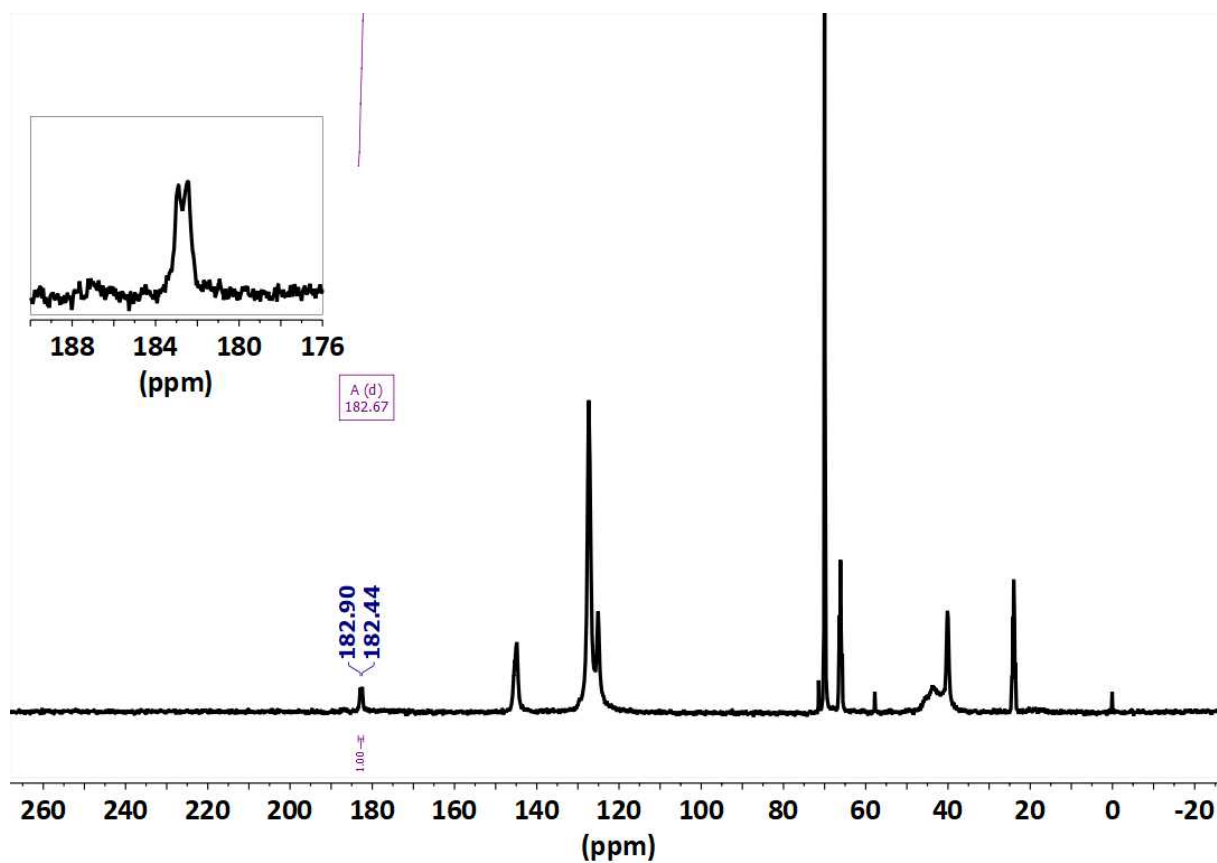
^1H -DFSE MAS (blue) and ^1H -MAS (black) NMR spectra of nanoreactors Rh-NHC^{mes}@CCM **5b***



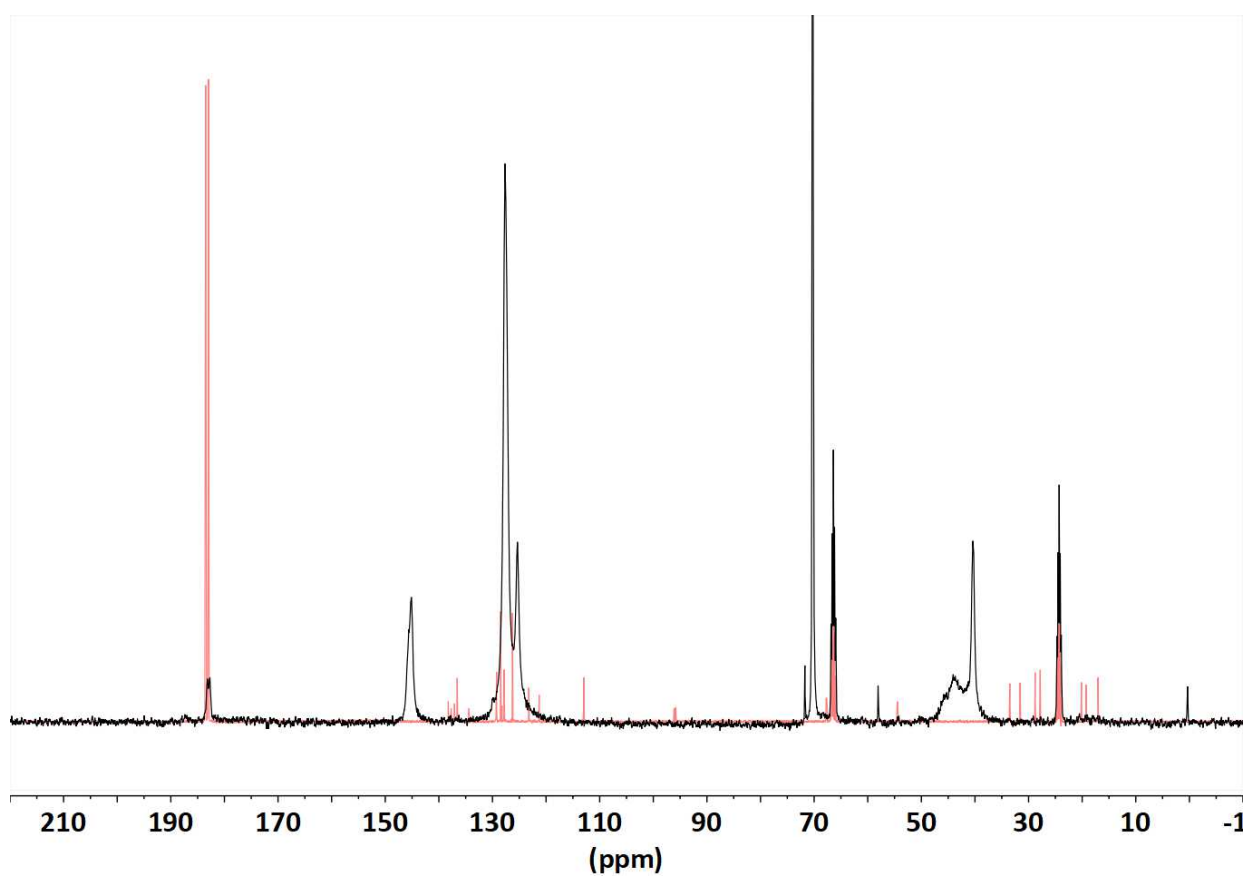
^1H -DFSE MAS NMR spectrum of nanoreactors Rh-NHC^{mes}@CCM **5b*** (black) and ^1H NMR spectrum of ^{13}C -labelled polymerizable rhodium(I) complex **2b*** (THF-*d*₈) (red)



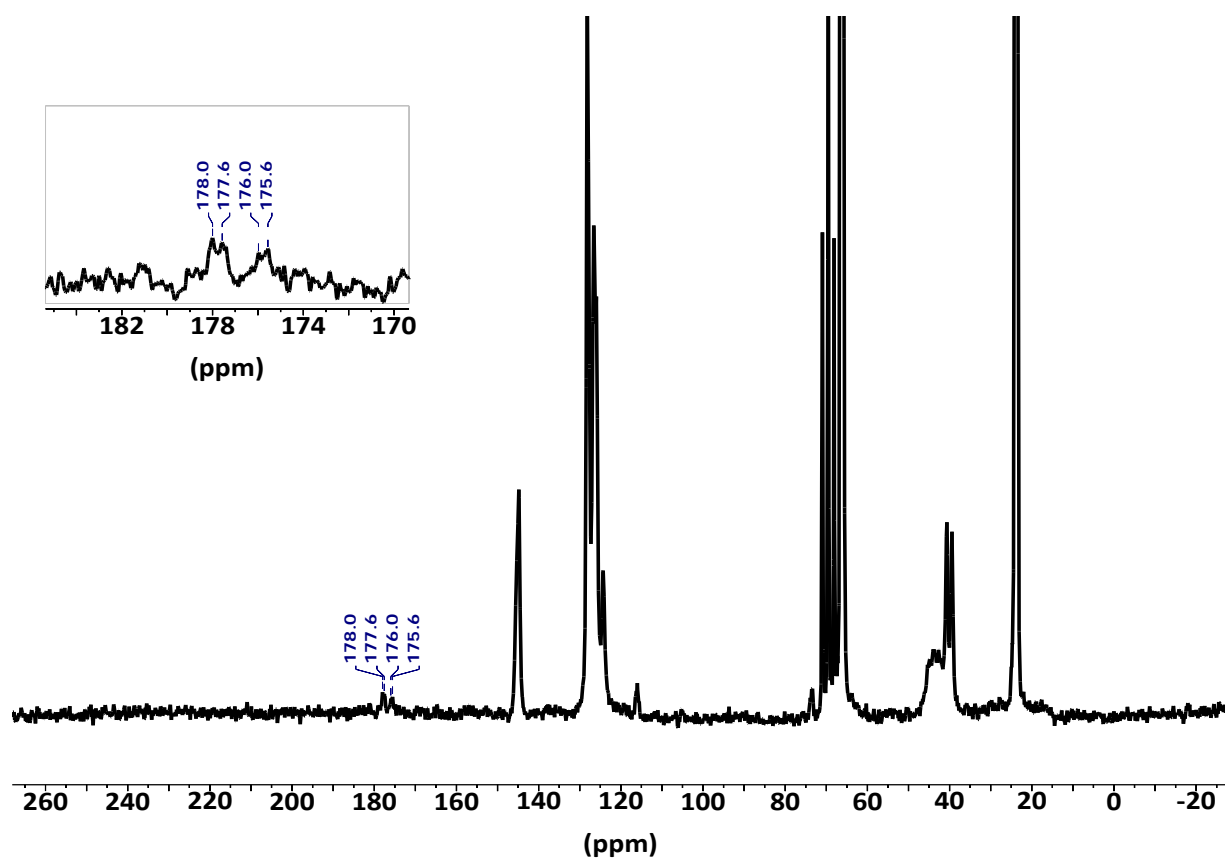
^{13}C -MAS NMR spectrum of nanoreactors Rh-NHC^{mes}@CCM **5b***



^{13}C -MAS NMR spectrum of nanoreactors Rh-NHC^{mes}@CCM **5b*** (black) and ^{13}C NMR spectrum of ^{13}C -labelled polymerizable rhodium(I) complex **2b*** (THF-*d*₈) (red)

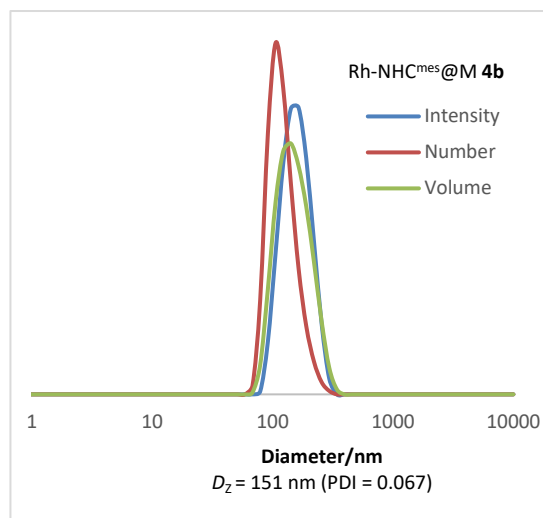
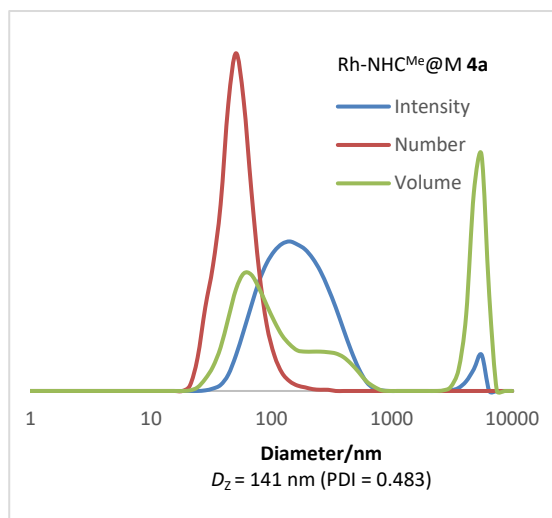


^{13}C -MAS NMR spectrum of nanoreactors Rh-NHC^{mes}@CCM **5b*** recovered after 5 runs hydrogenation.

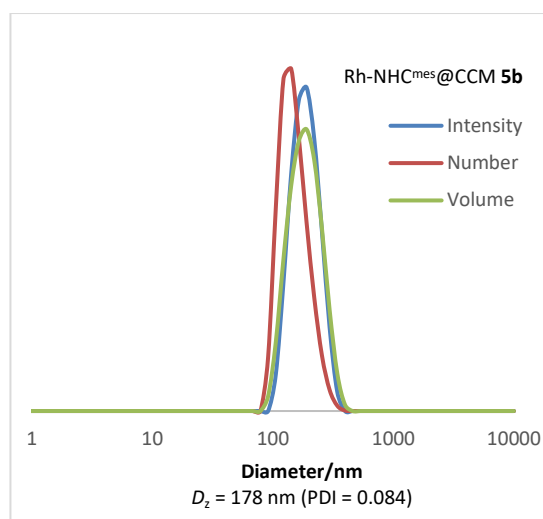
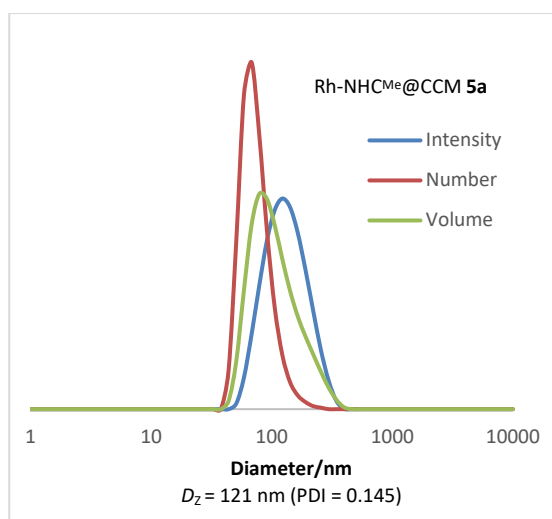


DLS analyses

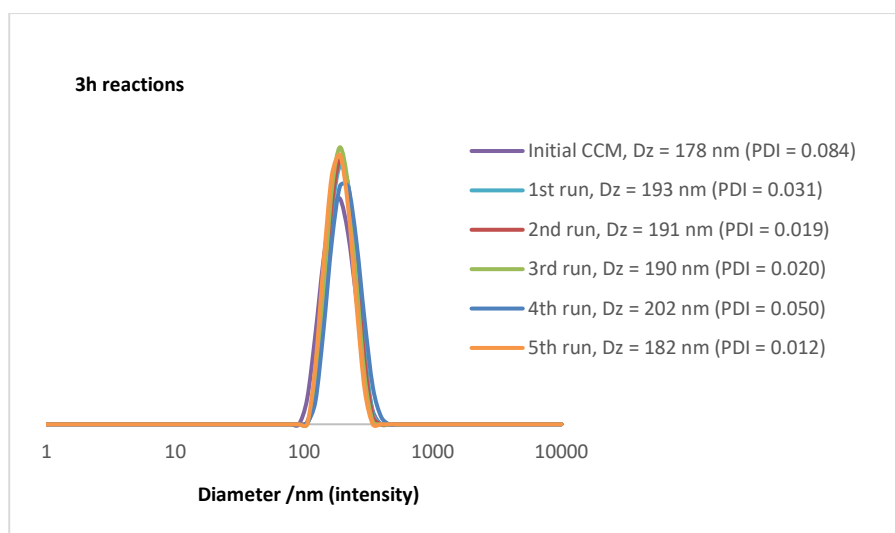
DLS analyses of Rh-NHC^{Me}@M **4a** (left) and Rh-NHC^{mes}@M **4b** (right), 45 μm filter



DLS analyses of Rh-NHC^{Me}@CCM **5a** (left) and Rh-NHC^{mes}@CCM **5b** (right), 45 μm filter

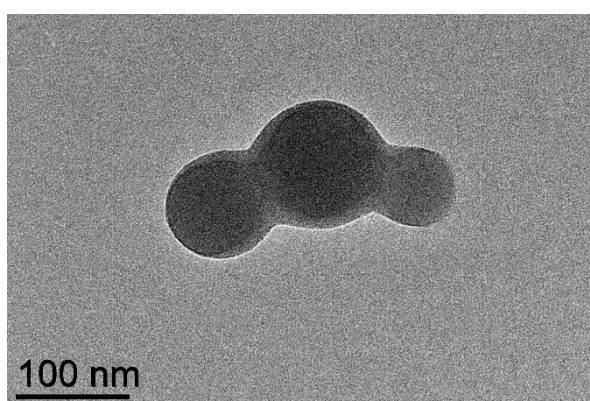
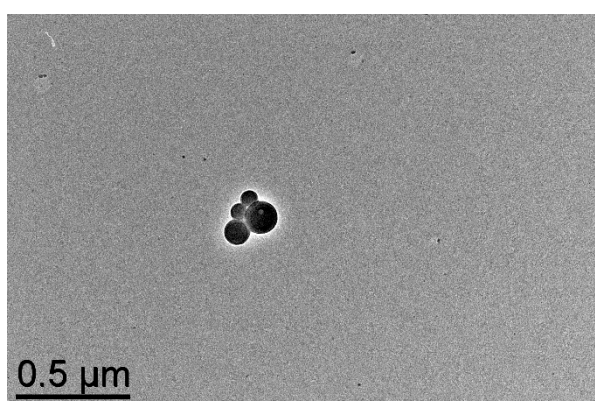
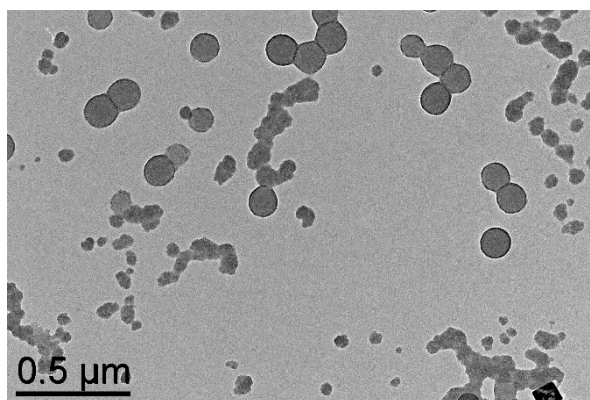
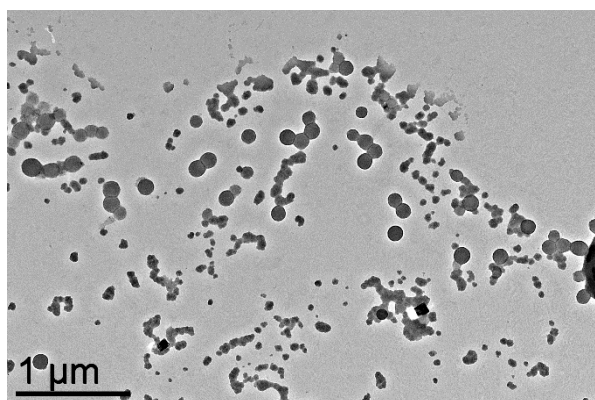


DLS analyses of Rh-NHC^{mes}@CCM **5b** after hydrogenation, 10 000/1 Sty/Rh ratio, 45 μm filter

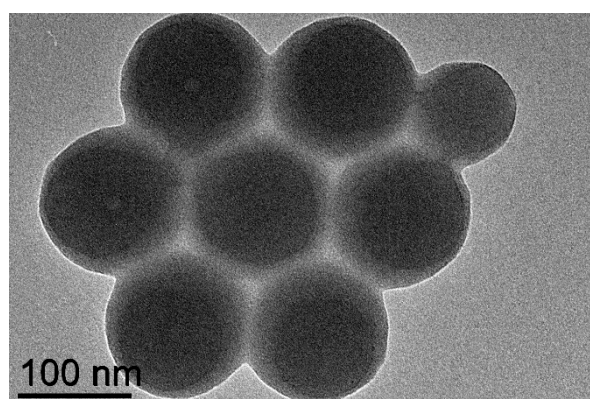
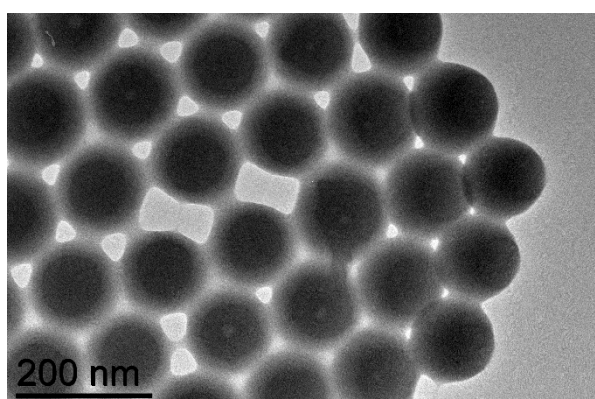
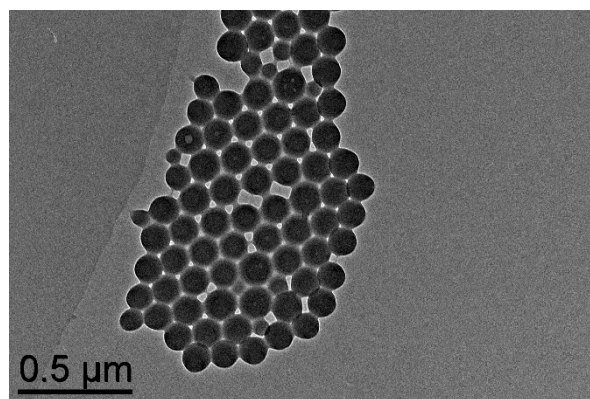
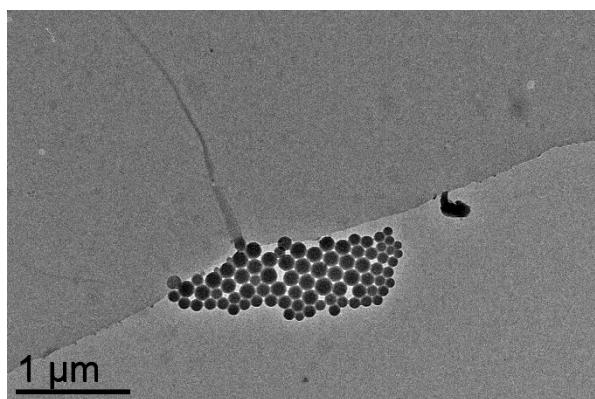


TEM analyses

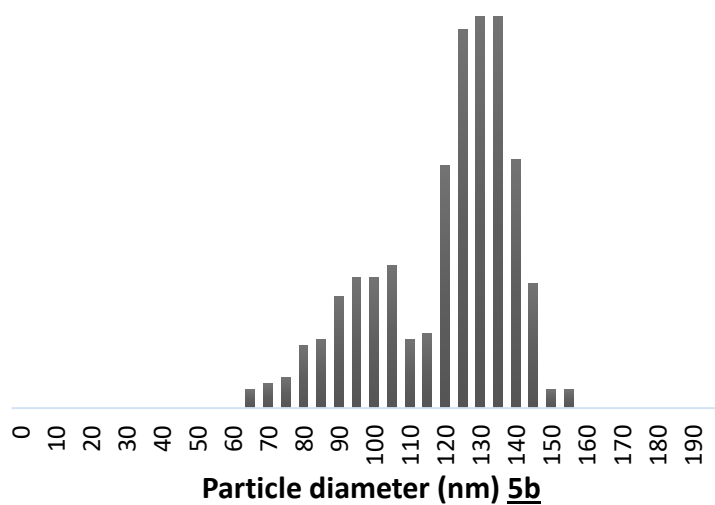
TEM images of Rh-NHC^{mes}@M **4b**:



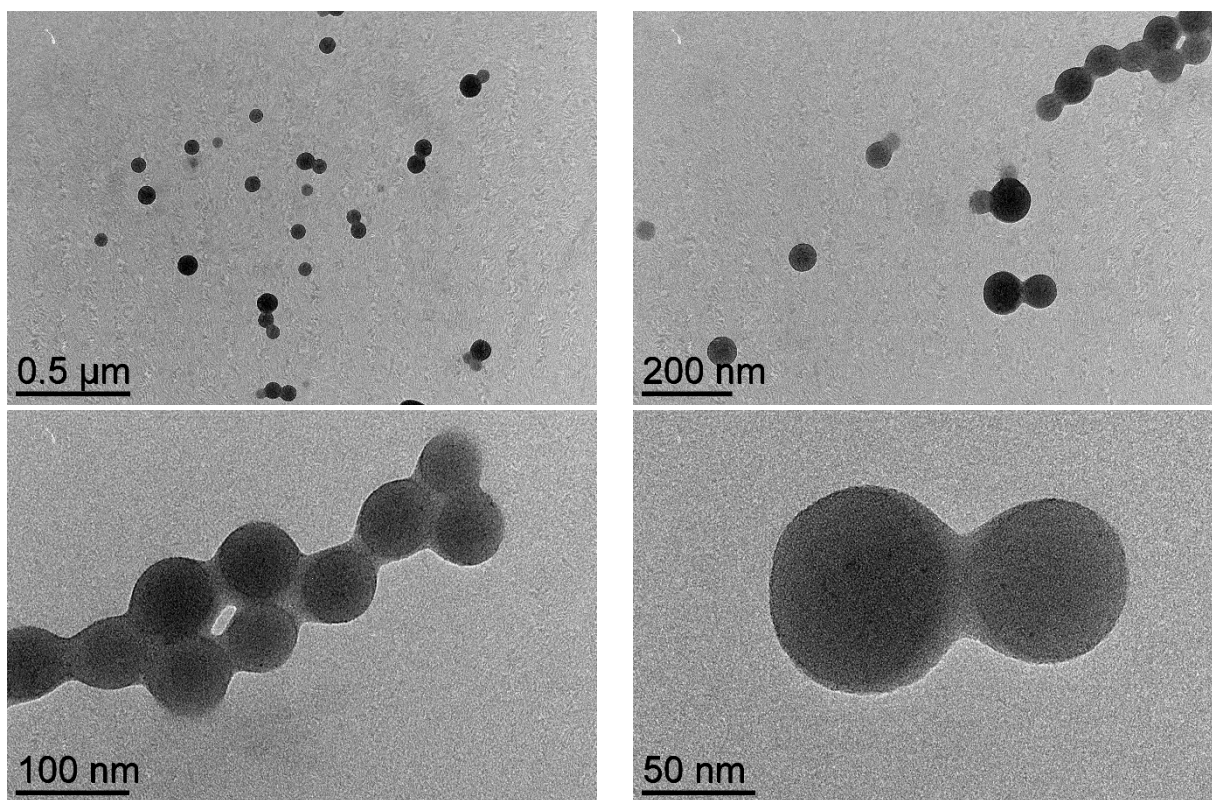
TEM images of Rh-NHC^{mes}@CCM **5b**:



Size distribution of Rh-NHC^{mes}@CCM **5b** measured on 431 particles, mean diameter: 123.3 ± 19.2 nm



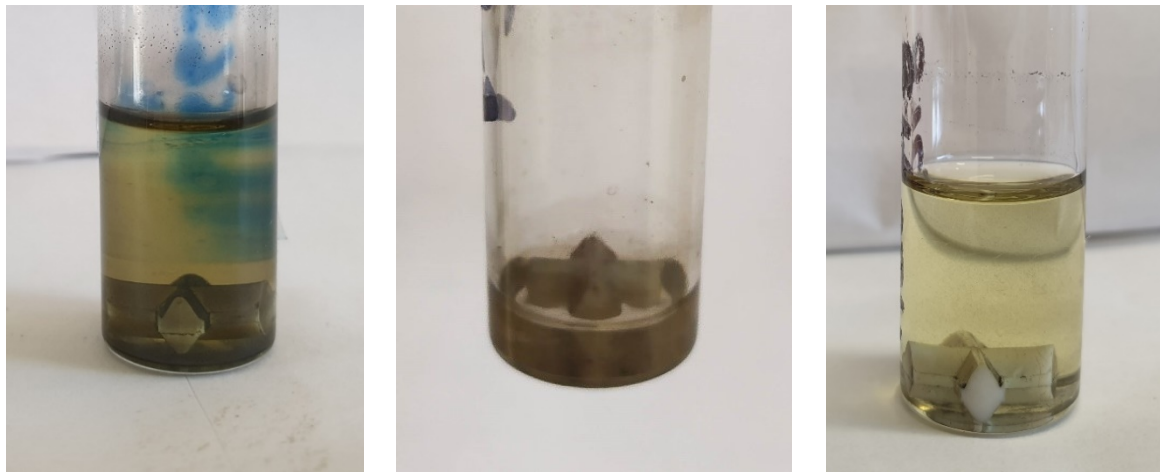
TEM images of Rh-NHC^{mes}@CCM **5b*** after 5 hydrogenation runs:



Photos of catalytic mixtures after hydrogenation

The reactions were carried out at a 1000/1 styrene/Rh ratio, 6h at 80°C, 20 bar H₂.

Reaction mixtures with **7b** under “wet toluene” conditions (left), “on-water” conditions (middle) or toluene/DME 1:1 conditions (right):



Biphasic mixture with **7b** incorporated into “blank” (non-functionalized polystyrene core) CCMs: “blank” CCMs + **7b** (aqueous phase) + styrene/toluene solution, after 1 run hydrogenation.



Aqueous phases containing **5b***, recovered after 1 run (left) and after 5 runs/4 recycles (right).



X-Ray diffraction analyses

Table 1. Crystal data and structure refinement.

Identification code	2a	2b
Empirical formula	C ₂₁ H ₂₆ Cl N ₂ Rh	C ₂₉ H ₃₄ Cl N ₂ Rh
Formula weight	444.80	548.94
Temperature, K	173(2)	173(2)
Wavelength, Å	1.54184	0.71073
Crystal system	Monoclinic	Monoclinic
Space group	P 2 ₁ /n	P 2 ₁ /c
a, Å	12.4856(3)	17.8663(7)
b, Å	10.6263(2)	15.7110(6)
c, Å	15.2385(4)	9.4111(4)
α, °	90.0	90.0
β, °	98.181(2)	96.939(4)
γ, °	90.0	90.0
Volume, Å ³	2001.20(8)	2622.32(18)
Z	4	4
Density (calc), Mg/m ³	1.476	1.390
Abs. coefficient, mm ⁻¹	8.153	0.772
F(000)	912	1136
Crystal size, mm ³	0.500 x 0.270 x 0.050	0.5 x 0.35 x 0.1
Theta range, °	4.290 to 61.163	2.891 to 26.371°
Reflections collected	9274	36687
Indpt reflections (R _{int})	3054 (0.0333)	5344 (0.1512)
Absorption correction	Sphere	Multiscan
Max. / min. transmission	0.10401 and 0.03020	0.7461 / 0.6609
Refinement method	F ²	F ²
Data /restraints/parameters	3054 / 0 / 227	5344 / 20 / 359
Goodness-of-fit on F ²	1.045	1.206
R1, wR2 [I>2σ(I)]	0.0378, 0.1002	0.0518, 0.1011
R1, wR2 (all data)	0.0411, 0.1045	0.0542, 0.1024
Residual density, e.Å ⁻³	1.239 / -0.299	0.529 / -0.901

Table 2. Bond lengths [Å] and angles [°] for **2a**.

Rh(1)-Cl(1)	2.3763(10)	Rh(1)-C(1)	2.030(4)
Rh(1)-C(11)	2.200(4)	Rh(1)-C(15)	2.105(4)
Rh(1)-C(12)	2.189(4)	Rh(1)-C(16)	2.095(4)
N(2)-C(1)	1.353(5)	N(5)-C(1)	1.350(5)
N(2)-C(3)	1.377(5)	N(5)-C(4)	1.374(5)
N(2)-C(21)	1.462(5)	N(5)-C(51)	1.474(5)
C(11)-C(12)	1.382(6)	C(14)-C(15)	1.532(6)
C(11)-C(18)	1.508(7)	C(15)-C(16)	1.413(6)
C(12)-C(13)	1.498(7)	C(16)-C(17)	1.520(7)
C(13)-C(14)	1.529(7)	C(17)-C(18)	1.510(8)
C(3)-C(4)	1.336(6)	C(54)-C(55)	1.396(7)
C(51)-C(52)	1.505(6)	C(55)-C(56)	1.388(7)
C(52)-C(57)	1.382(6)	C(55)-C(58)	1.473(7)
C(52)-C(53)	1.399(6)	C(56)-C(57)	1.383(7)
C(53)-C(54)	1.370(7)	C(58)-C(59)	1.311(9)

C(11)-Rh(1)-Cl(1)	93.65(14)	C(12)-Rh(1)-Cl(1)	89.40(13)
C(1)-Rh(1)-C(11)	162.78(16)	C(1)-Rh(1)-C(12)	160.44(15)
C(1)-Rh(1)-C(15)	92.28(16)	C(1)-Rh(1)-C(16)	90.07(17)
C(15)-Rh(1)-Cl(1)	160.17(12)	C(16)-Rh(1)-Cl(1)	160.49(12)
C(15)-Rh(1)-C(12)	82.50(17)	C(16)-Rh(1)-C(12)	97.49(18)
C(16)-Rh(1)-C(11)	81.47(19)	C(15)-Rh(1)-C(11)	90.61(17)
C(1)-Rh(1)-Cl(1)	89.36(10)	N(5)-C(1)-N(2)	104.3(3)
C(1)-N(2)-C(3)	111.0(3)	C(1)-N(5)-C(4)	111.0(3)
C(1)-N(2)-C(21)	124.8(3)	C(1)-N(5)-C(51)	124.0(3)
C(3)-N(2)-C(21)	124.1(3)	C(4)-N(5)-C(51)	125.0(3)
N(2)-C(1)-Rh(1)	128.4(3)	N(5)-C(1)-Rh(1)	127.3(3)
C(4)-C(3)-N(2)	106.7(3)	C(3)-C(4)-N(5)	107.1(3)
C(12)-C(11)-C(18)	123.6(4)	C(57)-C(52)-C(51)	122.2(4)
C(11)-C(12)-C(13)	126.2(4)	C(53)-C(52)-C(51)	119.6(4)
C(12)-C(13)-C(14)	114.0(4)	C(54)-C(53)-C(52)	121.4(4)
C(13)-C(14)-C(15)	113.5(4)	C(53)-C(54)-C(55)	120.5(4)
C(16)-C(15)-C(14)	123.6(4)	C(56)-C(55)-C(54)	117.9(4)
C(15)-C(16)-C(17)	125.5(4)	C(56)-C(55)-C(58)	120.7(5)
C(18)-C(17)-C(16)	114.8(4)	C(54)-C(55)-C(58)	121.3(5)
C(11)-C(18)-C(17)	111.7(4)	C(57)-C(56)-C(55)	121.5(4)
N(5)-C(51)-C(52)	112.0(3)	C(52)-C(57)-C(56)	120.4(4)
C(57)-C(52)-C(53)	118.2(4)	C(59)-C(58)-C(55)	126.7(6)

Table 3. Bond lengths [Å] and angles [°] for **2b**.

Rh(1)-Cl(1)	2.3839(9)	Rh(1)-C(1)	2.034(3)
Rh(1)-C(12)	2.187(4)	Rh(1)-C(16)	2.096(3)
Rh(1)-C(11)	2.195(4)	Rh(1)-C(15)	2.095(4)
N(2)-C(1)	1.359(4)	N(5)-C(1)	1.351(4)
N(2)-C(3)	1.388(4)	N(5)-C(4)	1.381(5)
N(2)-C(21)	1.440(4)	N(5)-C(51)	1.459(5)
C(3)-C(4)	1.328(5)	C(21)-C(22)	1.386(4)
C(12)-C(11)	1.377(7)	C(21)-C(26)	1.387(5)
C(12)-C(13)	1.492(7)	C(22)-C(23)	1.384(5)
C(11)-C(18)	1.513(7)	C(22)-C(221)	1.489(5)
C(17)-C(18)	1.516(7)	C(23)-C(24)	1.378(5)
C(16)-C(17)	1.493(5)	C(24)-C(25)	1.377(5)
C(15)-C(16)	1.392(5)	C(24)-C(241)	1.510(5)
C(15)-C(14)	1.521(5)	C(25)-C(26)	1.393(5)
C(13)-C(14)	1.527(7)	C(26)-C(261)	1.504(5)
C(51)-C(52A)	1.508(6)	C(51)-C(52B)	1.508(6)
C(52A)-C(53A)	1.391(12)	C(52B)-C(53B)	1.361(12)
C(52A)-C(57A)	1.391(11)	C(52B)-C(57B)	1.415(12)
C(53A)-C(54A)	1.383(15)	C(53B)-C(54B)	1.388(15)
C(54A)-C(55A)	1.395(16)	C(54B)-C(55B)	1.388(17)
C(55A)-C(56A)	1.397(18)	C(55B)-C(56B)	1.399(18)
C(55A)-C(58A)	1.489(16)	C(55B)-C(58B)	1.468(14)
C(56A)-C(57A)	1.391(16)	C(56B)-C(57B)	1.381(16)
C(58A)-C(59A)	1.290(13)	C(58B)-C(59B)	1.289(14)

C(1)-Rh(1)-C(15)	96.54(13)	C(16)-Rh(1)-C(11)	81.00(16)
C(1)-Rh(1)-C(16)	92.29(13)	C(1)-Rh(1)-Cl(1)	87.78(10)
C(1)-Rh(1)-C(12)	162.34(16)	C(15)-Rh(1)-Cl(1)	157.49(11)
C(15)-Rh(1)-C(12)	81.72(16)	C(16)-Rh(1)-Cl(1)	163.48(11)
C(16)-Rh(1)-C(12)	97.02(15)	C(12)-Rh(1)-Cl(1)	87.50(12)
C(1)-Rh(1)-C(11)	160.86(15)	C(11)-Rh(1)-Cl(1)	93.63(12)
C(15)-Rh(1)-C(11)	89.44(15)	N(5)-C(1)-N(2)	103.7(3)
N(2)-C(1)-Rh(1)	129.9(2)	N(5)-C(1)-Rh(1)	125.9(2)
C(1)-N(2)-C(3)	110.9(3)	C(1)-N(5)-C(4)	111.7(3)
C(1)-N(2)-C(21)	125.6(3)	C(1)-N(5)-C(51)	123.3(3)
C(3)-N(2)-C(21)	123.4(3)	C(4)-N(5)-C(51)	124.6(3)
C(4)-C(3)-N(2)	107.0(3)	C(3)-C(4)-N(5)	106.7(3)

C(12)-C(11)-C(18)	123.9(4)	C(16)-C(15)-C(14)	124.1(4)
C(11)-C(18)-C(17)	112.8(3)	C(15)-C(14)-C(13)	112.7(4)
C(16)-C(17)-C(18)	113.0(4)	C(12)-C(13)-C(14)	113.4(4)
C(15)-C(16)-C(17)	126.5(3)		
C(22)-C(21)-N(2)	119.5(3)	C(26)-C(21)-N(2)	118.2(3)
C(22)-C(21)-C(26)	122.3(3)	C(25)-C(24)-C(241)	121.4(4)
C(23)-C(22)-C(21)	117.6(3)	C(23)-C(24)-C(241)	120.4(4)
C(23)-C(22)-C(221)	120.6(3)	C(24)-C(25)-C(26)	122.0(3)
C(21)-C(22)-C(221)	121.7(3)	C(21)-C(26)-C(25)	117.4(3)
C(24)-C(23)-C(22)	122.3(3)	C(21)-C(26)-C(261)	122.2(3)
C(25)-C(24)-C(23)	118.3(3)	C(25)-C(26)-C(261)	120.4(3)
N(5)-C(51)-C(52B)	111.6(3)	C(59A)-C(58A)-C(55A)	127.3(15)
N(5)-C(51)-C(52A)	111.6(3)	C(53B)-C(52B)-C(57B)	121.4(10)
C(53A)-C(52A)-C(57A)	114.6(10)	C(53B)-C(52B)-C(51)	126.2(8)
C(53A)-C(52A)-C(51)	120.0(7)	C(57B)-C(52B)-C(51)	112.4(8)
C(57A)-C(52A)-C(51)	125.4(8)	C(52B)-C(53B)-C(54B)	117.8(14)
C(54A)-C(53A)-C(52A)	123.6(15)	C(53B)-C(54B)-C(55B)	120.4(15)
C(53A)-C(54A)-C(55A)	121.0(16)	C(54B)-C(55B)-C(56B)	117.9(12)
C(54A)-C(55A)-C(56A)	113.5(12)	C(54B)-C(55B)-C(58B)	121.1(15)
C(54A)-C(55A)-C(58A)	121.9(14)	C(56B)-C(55B)-C(58B)	118.5(16)
C(56A)-C(55A)-C(58A)	123.4(14)	C(57B)-C(56B)-C(55B)	119.3(15)
C(57A)-C(56A)-C(55A)	124.0(13)	C(56B)-C(57B)-C(52B)	119.1(14)
C(56A)-C(57A)-C(52A)	121.1(13)	C(59B)-C(58B)-C(55B)	126.6(15)